Applications Of Blockchain Technology To Distributed Computing In High Energy Physics

Joseph C Wang (joequant@bitquant.com.hk)
Bitquant Digital Services (Hong Kong)

2024 International Workshop on the High Energy Circular Electron Positron Collider
Poster Id: 29

Abstract

The HEP software community has identified scalability, complexity, and cost as barriers to advancing high-performance computing in high-energy physics. We intend to address these issues by pulling technology from other domains, such as artificial intelligence, traditional financial technology, web3, and blockchain. By combining computational systems from other domains with existing HEP software, the HEP software community can share costs, pool resources, and aggregate computation power with other computational domains addressing these issues.

In this poster, we will describe the current status and design of our blockchain system which leverages existing open source software technology and web3 for generalized high-performance computing and its application to high energy physics and AI. Our computational infrastructure using comprises a decentralized blockchain system that passes messages between computational nodes, implemented as docker/OCI containers. We use an the end-to-end principle to place policy controls at the endpoints, drastically simplifying computational complexity and removing barriers to international resource sharing between institutions and professional domains.

To support HEP workflows, we are integrating the streaming network with a computational node that uses the KEY4HEP framework to include software commonly used in HEP, such as ROOT, Gaudi, and Podio. We have designed the system to allow easy integration with software-as-a-service systems such as AI providers such as ChatGPT or OpenLlama. We have designed the system to be scalable both upward, allowing the creation of computational networks of the scale of the Bitcoin computation network, and downward, allowing the creation of simple ad hoc distributed computation systems. An open-source prototype of our work is available on GitHub, and we are seeking users and developers from the HEP community.

Motivation

The motivation for this project is to apply high performance computing in quantitative finance and cryptocurrency mining to high performance computing problems. The typical investment bank has a team of several hundred people (half with STEM Ph.D.'s) doing quantitative finance.In the cryptocurrency world, there are vast networks of computing systems that are doing cryptocurrency mining.

Communities

The project will need to combine expertise and systems from three different communities, and will use Hong Kong has a location to connect these three communities

- HEP Physics - The HEP physics needs large amount of computing power and tools to allow quick and easy use of computational resources. There is also the need for funding for development. HEP prioritized working systems and dislikes hype and future promises.
- Traditional quantitative finance - In traditional quantitative finance there is the need to do complex mathematical calculations to run banks. This sector has a lot of funding resources, and project funding is based on regulatory needs (i.e. regulator stress tests). Technical knowledge very high as many people in this field have STEM backgrounds.
- Cryptocurrency - This community is interested in creating the next big thing. There are people with funding resources but funders often have uneven levels of technical expertise, but resources are allocated based on hype and spin. Operating massive clusters of computer system. Bitcoin is the world's biggest and most inefficient computer systems. Because the goal is making money and not technology, the incentives are that often projects with little or no merit are being funded

Architecture and Implementation

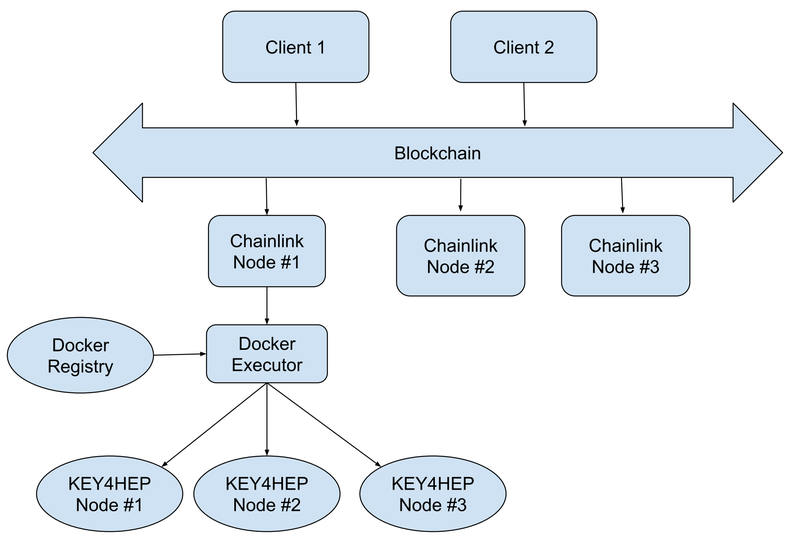

Blockchains have high latency and low speed message passing. Typical speed is one message every ten seconds. However, goal is to compensate with low latency by high parallelization Need scalability going up and down. The architecture will bootstrap the system with small clusters and then link the clusters worldwide

In response to messages sent down the database, the server will execute a docker container using KEY4HEP distribution then using the blockchain to send commands to run the software. Different domains can have different software packages and compute nodes, and the benefit is with having a global blockchain is that you can then send messages between different domains.

Current Status

- All source code available on github via open source license
- Now creating simple proof of concept with KEY4HEP calculation node and connecting to blockchain via Chainlink server
- Thinking about security and authentication
- Use a local blockchain for small scale physics calculations and then scale upward

Target workflow modes

- Run the same calculation across multiple nodes to see if the calculation is correct. This is the typical mode for bitcoin which is the world's largest computational network, but the world's stre inefficient computational network
- Run different calculations are performed on different nodes (monte carlo calculations and parameter searches)

Example problems

- Parameter searches - Parallel computations across a large dimensional space - Optimization, Monte carlo and diffusion process with complex dynamics
- AI searches - Run problem against large numbers of AI models and choose the "best" answer
- GPU resource allocations - AI workflows require dedicated allocation of memory bandwidth to problems
- FPGA / Quantum computing - Once you abstract the calculation node then you can replace with quantum optimization system or dedicated hardware computation node

Access control and resource management

Access and resource management will be layered on top of the message passing system. We are working on basic infrastructure and will work on access and resource management later. In a blockchain system, each job and each computation node will have its own private key, and blockchains have mechanisms for sending a message on the network, and the ability to charge for computation.

Contact

Source code available at:
https://github.com/joequant/blockchain-hpc

Wechat - joequant

Telegram - joequanthk

Whatsapp - +852 6352 9195

Poster ID: 35

Investigating Beam Backgrounds in TPC and Developing Pixelated TPC Prototype for CEPC

Liwen YU [1] **Jinxian Zhang** [2] **Xin She** [2] **Yue Chang** [3] Zhi Deng [4] **Huirong Qi** [2] Linghui Wu [2]
Guang Zhao [2] Gang Li [2] Mingshui Chen [2] Jian Zhang [2] Jianchun Wang [2] Yifang Wang [2]
Manqi Ruan [2] Haoyu Shi [2] Canwen Liu [4] Jianmeng Dong [4]

[1]Fudan University [2]Institute of High Energy Physics, CAS [3]Nankai University [4]Tsinghua University

Introduction

In the latest design of the Circular Electron-Positron Collider (CEPC) detector, the time projection chamber (TPC) has been chosen as the main tracker detector (MTK). As shown in Fig. 1, a cylindrical drift volume with an inner radius of 0.6 m, an outer radius of 1.8 m, and a half-length of 2.9 m. This design aims to enhance the tracking acceptance ($\cos\theta \sim 0.98$) and provide thousands of 3D measurement points of charged tracks using 500 μm × 500 μm pixel readout.

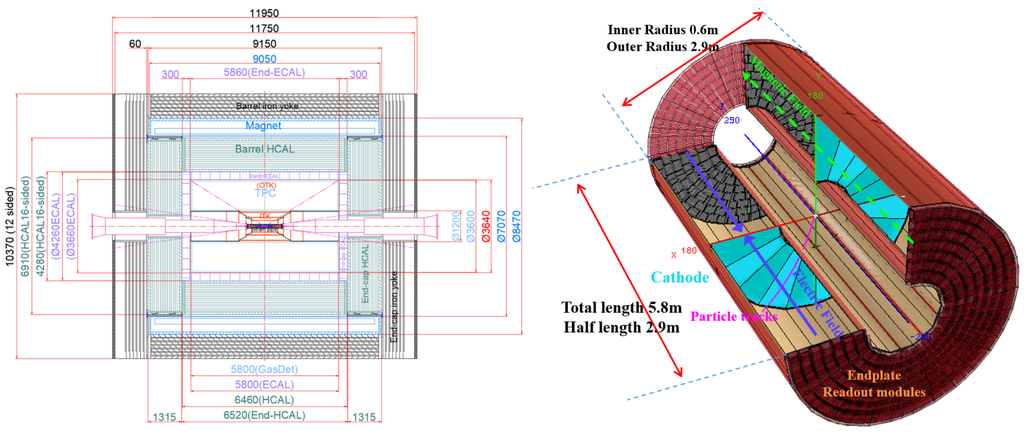

Figure 1. The detector layout of CEPC Ref-TDR (left) and The geometry of TPC at 3-D view (Right)

The TPC using high granularity pixel readout can provide up to thousands of 3-D space points, with a single hit resolution of approximately 100 μm in the r-φ plane, and it will be a promising technology, especially at the high luminosity Z-pole. In this poster, we will present the feasibility and progress of the high-precision TPC technology for CEPC and outline the next steps for developing pixelated TPC detector for CEPC Physics and Detector TDR.

Investigation of beam backgrounds in TPC

Under the CEPC different operation modes, it will produce massive quantity hits and ions in TPC drift volume, including physics events and beam backgrounds. Correspondingly, the TPC as a tracker detector needs to provide perfect position resolution and handle a high count rate. As shown in Fig. 2, the ions in TPC volume can be generated by the following three different processes:

- **Physics events:** $H \to ss/cc/sb, Z \to q\bar{q}$ ...(high P_T)
- **Beam Backgrounds:** Beamstrahlung (luminosity related), Touschek scattering, Beam-Gas ...
- **Ion back flow from the MPGD readout modules**

Beamstrahlung is one of the most important sources of beam-induced background. There are about 1300/680 e^+e^- produced for Higgs/Z-pole mode in each bunch crossing (BX). It will interact with the beam pipe or other materials within the TPC. Thus, these secondary particles will incident TPC and cause large amounts of hits and positive ions that might degrade the TPC performance.

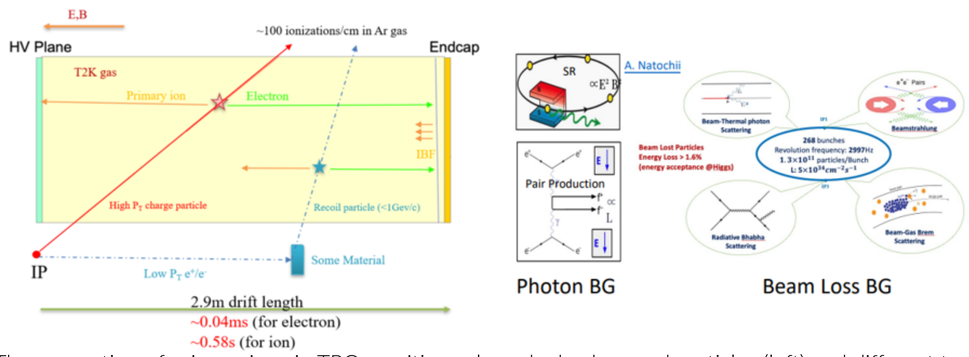

Figure 2. The generation of primary ions in TPC sensitive volume by background particles (left) and different types of beam backgrounds (Right)

A complete simulation flow was established to study the beamstrahlung and performance of TPC. 10000 BS files been simulated by Guinea-Pig++ and exported to CEPC Software (CEPCSW) for full detector simulation. Then, hits and energy deposits in TPC volume are extracted to evaluate the hit density and space charge distribution.

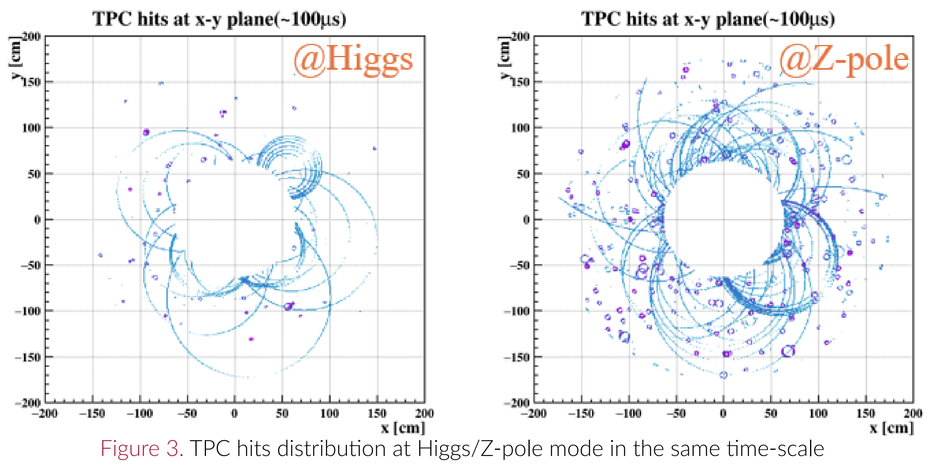

Figure 3. TPC hits distribution at Higgs/Z-pole mode in the same time-scale

Fig. 3 shows the TPC hits distribution caused by beamstrahlung at Higgs and Z-pole mode in the same time-scale. The hit density at Higgs mode is much lower than Z-pole due to smaller BX frequency. Detailed results about hit density and voxel occupancy at two operation mode are given in Table 1:

Table 1. Simulation result of hit density, VO and max. space charge density in TPC

Collider Detector Model	TDR_o1_v01	TDR_o1_v01
Beamstrahlung pairs	Z-pole(91GeV)	Higgs(240GeV)
BX freq.	1/23 ns	1/355 ns
Hit density [MHz/cm^2]	1.8	0.4
Voxel Occupancy	1.5×10^{-3}	2.8×10^{-4}
average primary ρ_{ion} [nC/m^3]	0.11	0.02
max (steady state) [nC/m^3]	0.32	0.06

Space charge effect and Distortion in TPC

The space charge density had been calculated from the hit density, weighted by the energy deposit. The distorted electric field caused by primary ions can be solved analytically based on Green's function.

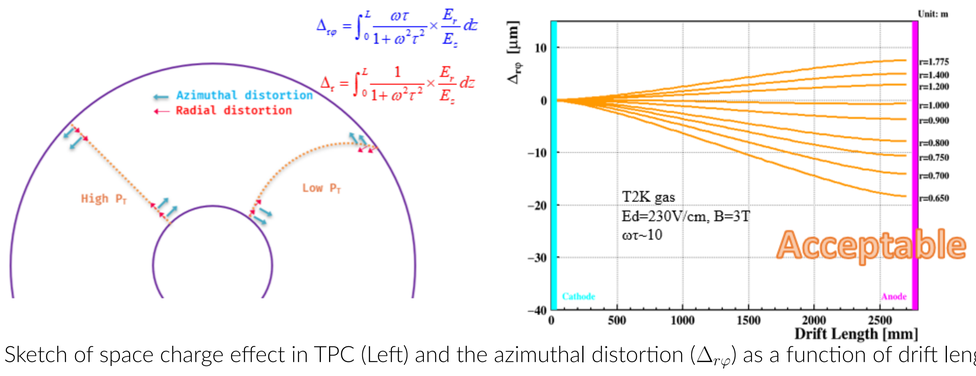

Figure 4. Sketch of space charge effect in TPC (Left) and the azimuthal distortion ($\Delta_{r\varphi}$) as a function of drift length (Right)

As shown in Figure 4, azimuthal distortion has more significant impact on both high/low P_T tracks compared to radial distortion. The maximum $\Delta_{r\varphi}$ is only $\sim$ 20 μm at Higgs mode, which is acceptable. However, the TPC performance will get $\sim$ ×5 degrade under Z-pole run, which needs further optimization on MDI design.

Developments of pixel TPC modules and prototype

In CEPC Ref-TDR, there are 248×2 readout modules at the TPC endplate. We have developed several TPC readout modules (See Fig. 5), glued with aluminum back frames, which can mounted in the large TPC prototype (LP) at DESY (see Fig. 6 right) and tested using electron beam.

Pixel TPC readout module

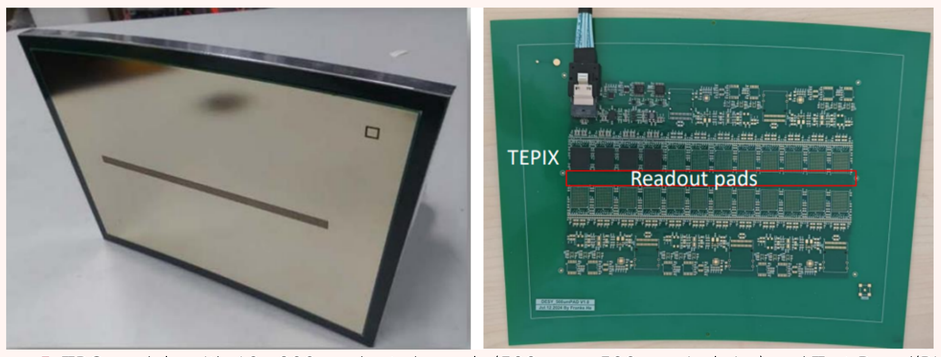

Figure 5. TPC module with 10×300 readout channels (500μm × 500μm pixel size) and Test Board(Right)

Pixel TPC prototype design and Large TPC prototype at DESY

Moreover, a small TPC prototype with 50 cm drift length has been designed (See in Fig. 6 left). The modules can also be installed at the endpalte for testing using 266 nm UV laser beam.

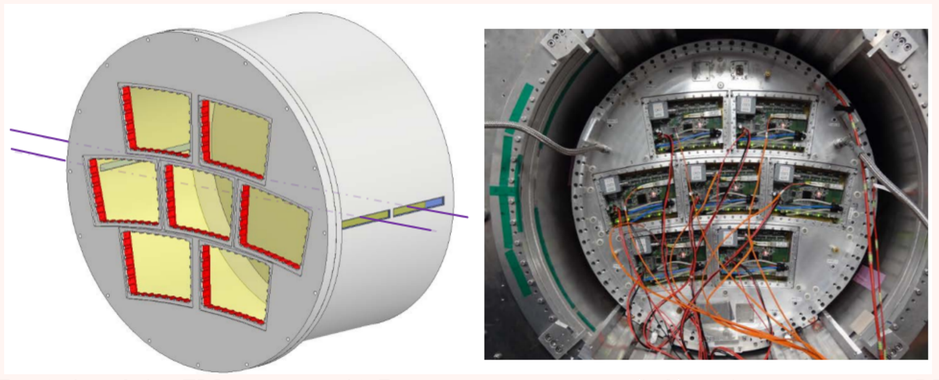

Figure 6. The design of pixel TPC prototype with 7 modules at the endplate (Left) and Large prototype at DESY (Right)

The 3000 channels will be connected to 24 low power consumption ASIC chips, named TEPIX, which is a particle detector readout chip with 128 channels for simultaneous energy and time measurements developed by Tsinghua University.

FEE ASIC chip test result and Offline analysis program:

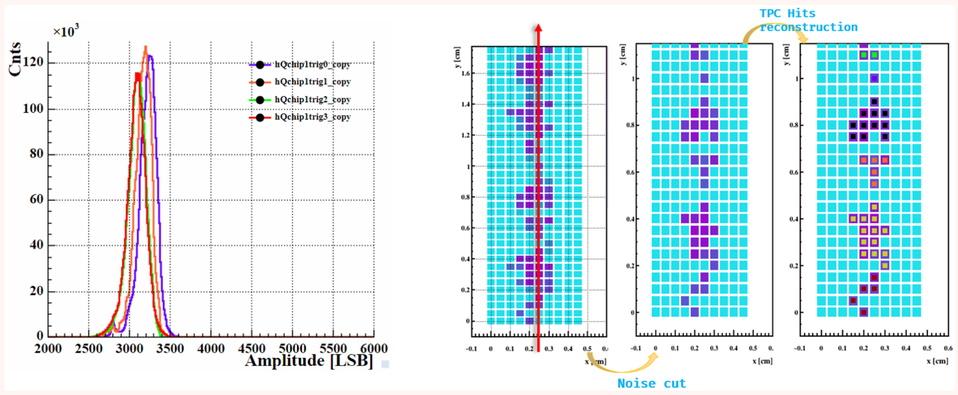

Figure 7. The amplitude distribution of TEPIX chips (Left) and diagram of the pixel TPC hit reconstruction process (Right)

- **Power consumption and Noise** $\sim$ 0.5 mW/ch, $\sim$ 300 e^-
- **Gain:** 314.2 LSB/fC
- **Get expected energy value according to the charge injected**. The Energy distributions of TEPIX chips are shown on Fig. 7 left.
- **Offline analysis program for pixel TPC prototype have been developed.** The **json** configuration file can be used to unpack the raw binary data, reconstruct TPC hits and tracks, etc. Fig. 7 right shows the diagram of hit reconstruction process.
- Beam test of the pixelated readout TPC prototype is underway in preparation. (November 2024 and January 2025)

Concusion

1. Pixel TPC can either operate at CEPC Higgs or high luminosity Z-pole mode based on full simulation results of beam backgrounds.
2. For the TPC modules and prototype R&D, readout modules assembled with TEPIX chips have been fabricated.
3. More detailed experimental studies using 266 nm UV laser and electron beams are ongoing.

Poster ID 46: Study of Synchrotron Background in the CEPC

Tang Yanbang
Email: tangyb@ihep.ac.cn

Introduction

The Circular Electron Positron Collider (CEPC) offers a significant opportunity to advance high-energy physics study. However, its operation also presents challenges related to synchrotron background radiation. Besides, the synchrotron radiation simulation software used during the CDR phase of the CEPC is no longer supported. Therefore, it is urgently necessary to develop a new synchrotron framework within this study. This study focuses on the characterization and mitigation of synchrotron background radiation within the CEPC accelerator environment. The results of this study aim to enhance the understanding of synchrotron radiation behavior within the CEPC and contribute to the development of effective mitigation strategies, thereby ensuring the optimal performance and longevity of the accelerator and its detectors.

Method

In this study, we utilized GEANT4, developed by CERN, to generate and track synchrotron radiation. The tracking results were then imported into CEPCSW, developed by IHEP, for detector simulations to quantify the impact of synchrotron radiation on various detectors within the MDI region. However, if the only purpose is to generate synchrotron radiation using GEANT4, constructing the complete CEPC lattice within a short period is both challenging and unnecessary. Therefore, this study is based on the design parameters of the CEPC—specifically, the deflection angle, the arc length of the deflection in the final dipole magnet upstream of the MDI region, and the electron energy—to calculate the absolute position and momentum direction of the incident electron as shown in Figure 1. These calculations will ensure that the incident electron, after being deflected by the final dipole magnet, reaches the beam pipe and continues its trajectory toward the MDI region. The synchrotron radiation generated under these deflection conditions is precisely the radiation required for this study.

In the subsequent work, we will use CEPCSW to simulate the distribution of synchrotron radiation photons in each detector to estimate the background level caused by synchrotron radiation.

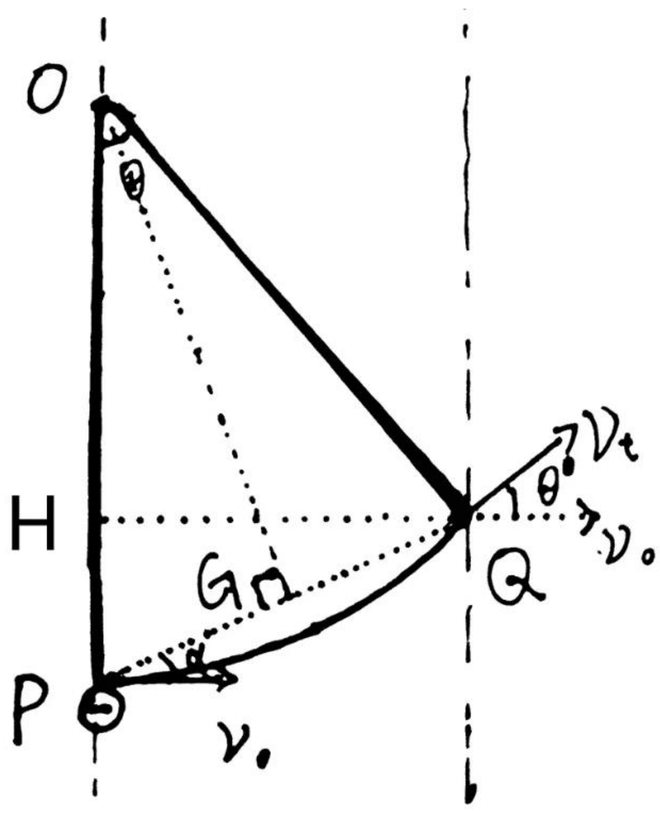

Figure 1. The theoretical sketch of the calculation of the electron source's incident parameters.

Result

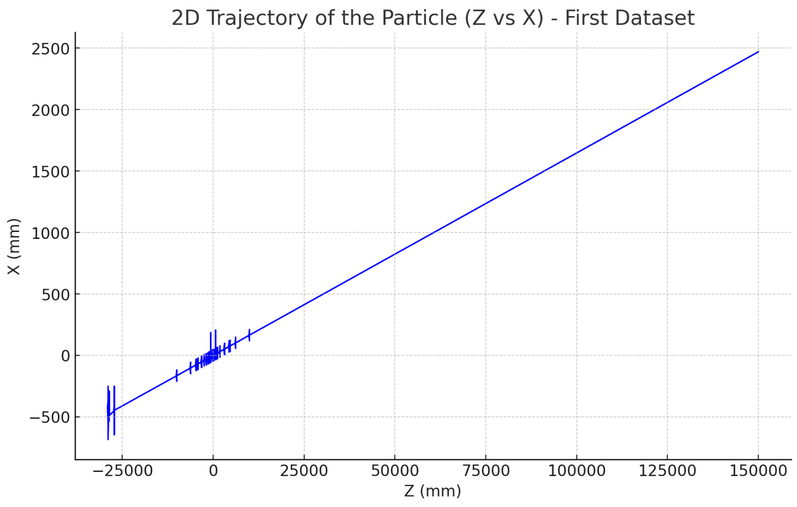

Figure 2. electron trajectories without dipole magnet

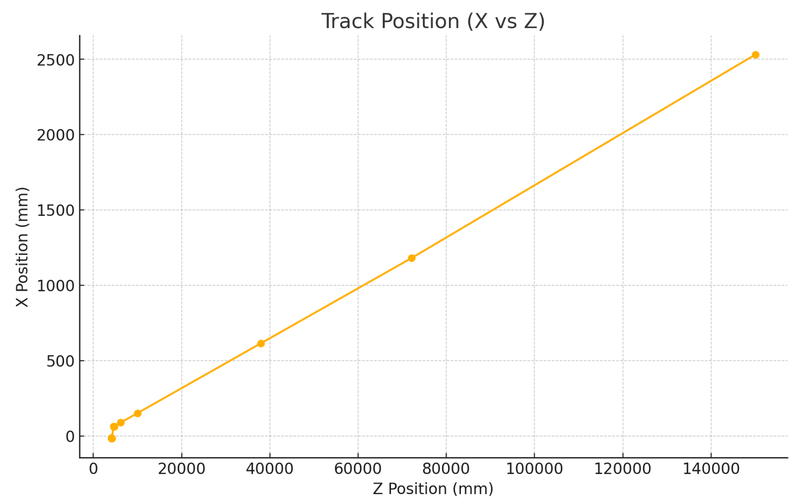

Figure 3. electron trajectories with dipole magnet

The above two figures show the electron trajectories without and with the dipole magnet, respectively. The fitted slope values of the curves are close to the crossing angle designed for the CEPC, and the recorded synchrotron radiation photons are also in the keV order of magnitude, which verifies the correctness of our synchrotron radiation generate method.

To simulate the actual operating conditions of the CEPC, where the number of particles per bunch (Num/bunch) can reach 10^{11}, parallel simulations for generator are performed by varying the random number seed. The results are subsequently combined into a single ROOT file for detector simulations using CEPCSW.

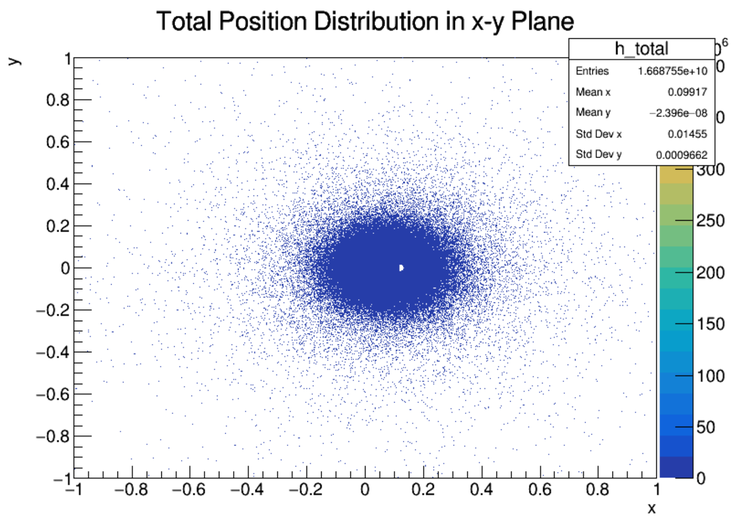

Figure 4. Distribution of synchrotron radiation

The above figure shows the distribution of synchrotron radiation photons at a distance of 7 meters upstream of IP. As seen in the figure, the photons are distributed over a large area, which could potentially cause irradiation and noise effects on various detectors in the MDI. Of course, this will depend on the final synchrotron radiation background results for each detector. If the impact is too significant, we will consider adding shielding walls to block synchrotron radiation photons from entering the detectors. The white spots in the figure are merely visual artifacts caused by the angle between the counting detector and the beam pipe in the software, and they do not affect the subsequent detector simulation results.

Summary and Outlook

This study successfully generated CEPC synchrotron radiation and tracked it through theoretical calculations and software simulations. The subsequent detector simulations are currently underway...

Reference List

[1] GEANT4 collaboration group.

[2] ROOT collaboration group.

[3] CDR of CEPC work group.

[4] CEPCSW work group.

Poster ID: 50

Radar, a DAQ software framework.

Xu Zhang

(1)University of Chinese Academy of Sciences, Beijing 100049, China
(2)State Key Laboratory of Particle Detection and Electronics, Institute of High Energy Physics, CAS, Beijing 100049, China

1.Introduction

- **ROS:** ReadOut System
- **DA:** Data Assemble
- **DP:** Data Processor
- **DS:** Data storage

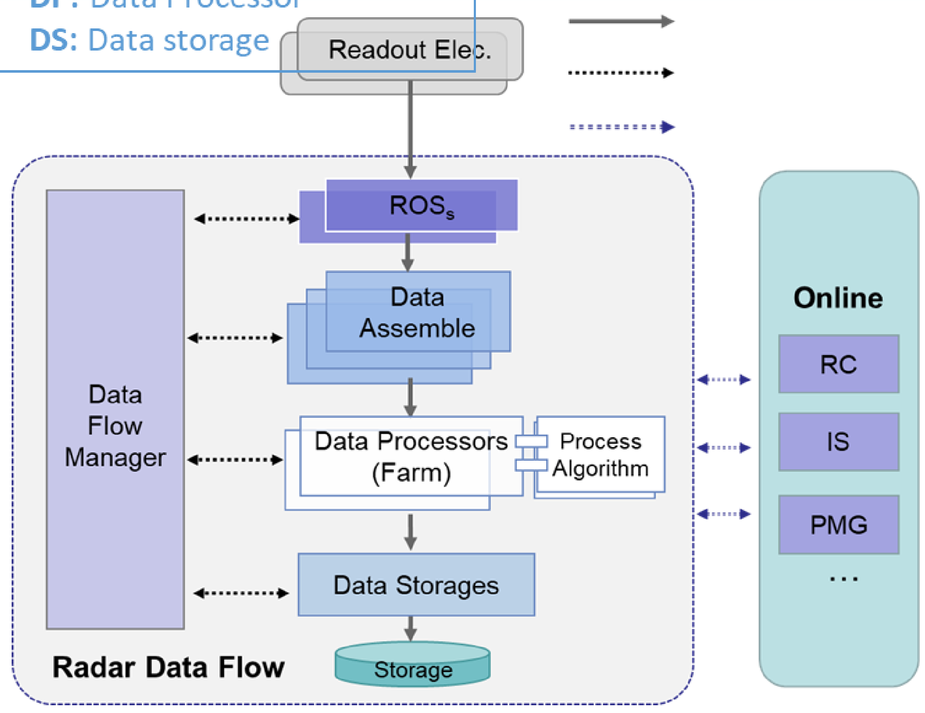

- **Radar**(heteRogeneous Architecture of Data Acquisition and pRocessing) is a software framework for high energy physics experiment data acquisition and online processing.
- The LHAASO DAQ and JUNO DAQ systems are developed based on RadarV1.0 and RadarV2.0, respectively.

2.Motivation

Resource consumption of JUNO

ROS Total CPU (cores)	DA Total CPU (cores)	DP Total CPU (cores)	DS Total CPU (cores)
1165 cores	47 cores	1026 cores	0.3 cores
ROS Total Memory	**DA Total Memory**	**DP Total Memory**	**DS Total Memory**
566 GiB	55 GiB	1632 GiB	2 GiB

~70Server Nodes, ~2000 valid CPU cores, for 40GB/s data.

Assuming that JUNO's data rate is 2 TB/s, the number of nodes used at this point goes up to 3500. We predict that CEPC will also use thousands of servers if it reuses RadarV2.0.

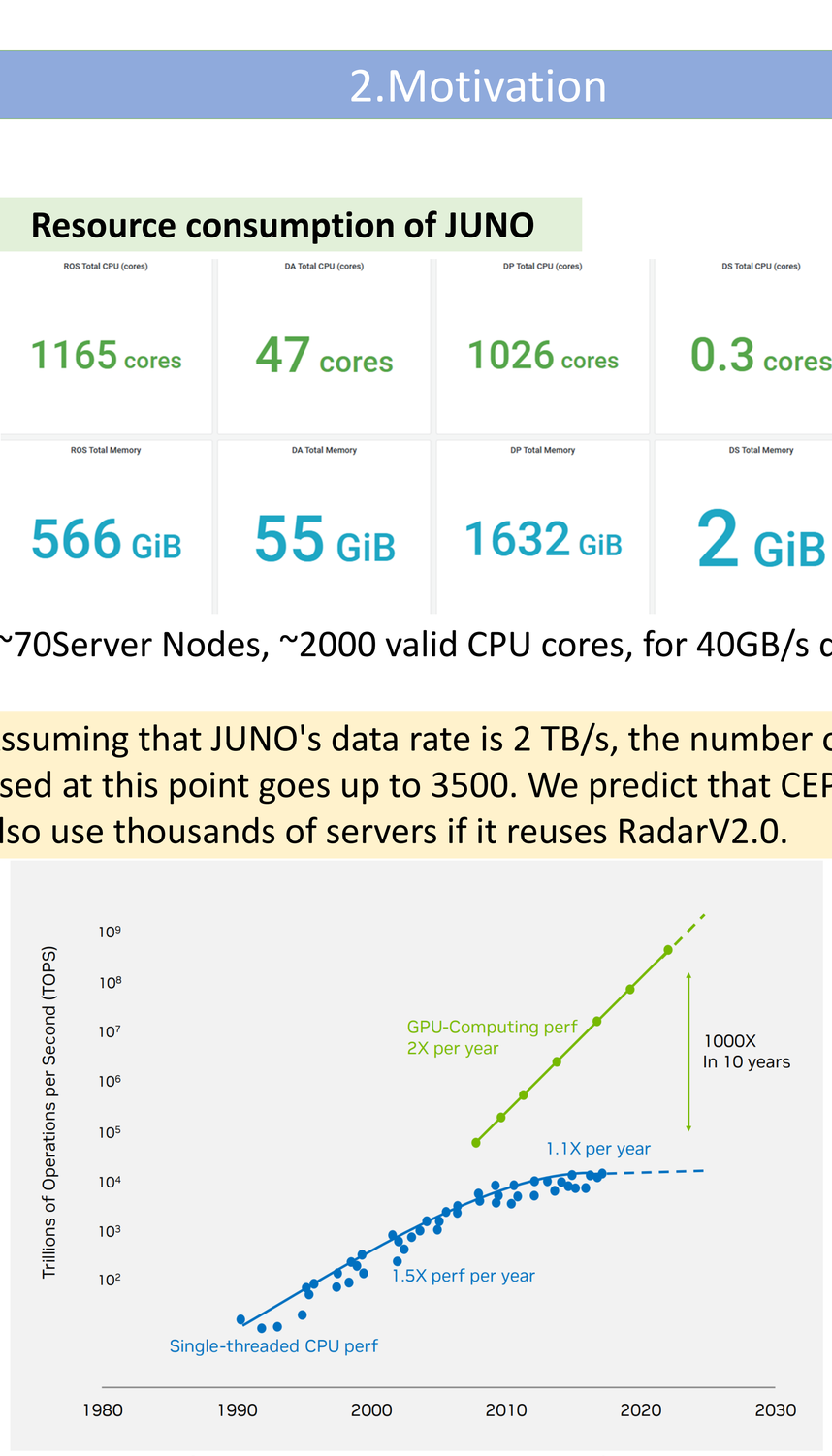

Ref: NVIDIA Investor Presentation. October 2022

Applying GPUs to improve computational performance on a single node.

- **GPUs have good potential.**
  GPU computing performance has increased 1000 times in the last 10 years.
- **GPUs can accelerate CEPC-related processing.**
  For example: Track reconstruction.

3. Architecture Design

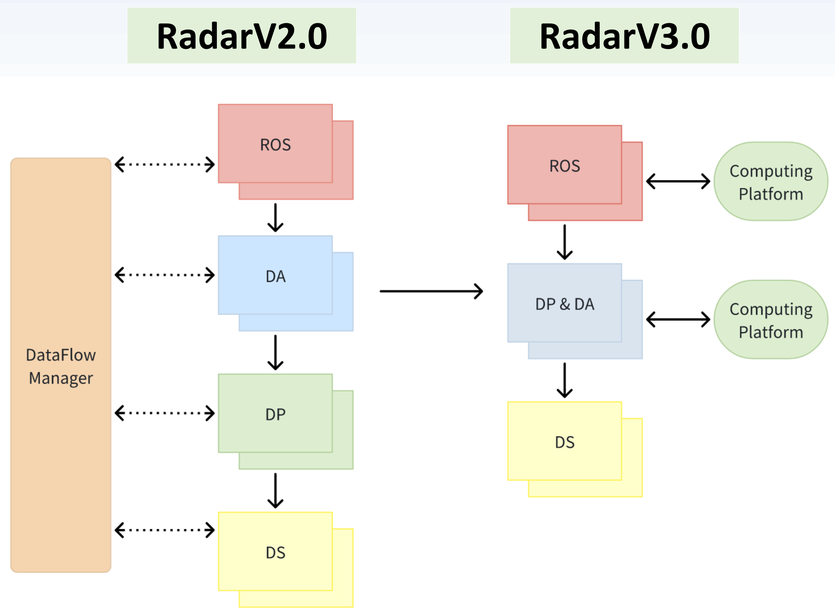

CEPC Requirement

8 Hz @Higgs 240GeV(50MW)
Bunch crossing rate: 2.889 MHz
82 kHz @Z pole 91GeV(50MW)
Bunch crossing rate: 43.3 MHz

CEPC has higher data rate, so RadarV3.0:

- Remove the DFM to increases the frequency of dispatch.
- Merge DA and DP reduces data transfer.
- Build **Heterogeneous Computing Platform** to Improve Computing Performance.

FPGA/GPU Computing Platform

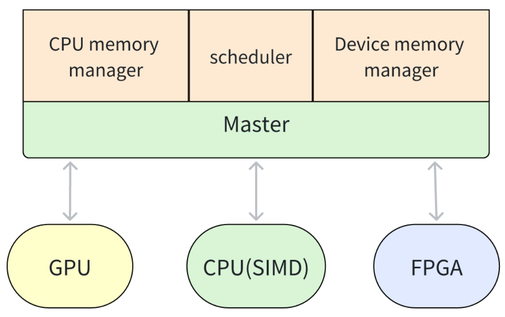

Select device based on task

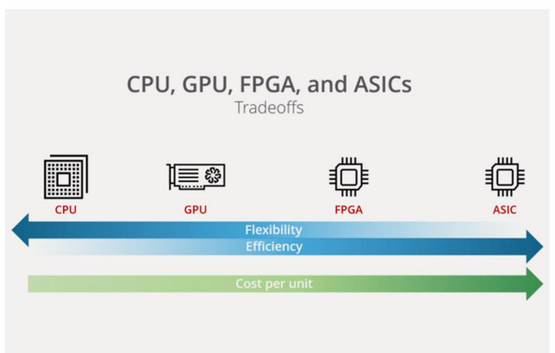

Ref:https://www.jiemian.com/article/5019639.html

- **Scheduler:** Assign algorithms to different devices and manage data transfer.
- **CPU Memory Manager:** Organizing parallel computing data structures.
- **Device Memory Manger:** Manage device memory for reducing data transfer.

4. Application Scenario

CEPC Requirement for TDAQ

Event Type	Data rate	Storage rate
Higgs	< TB/s	< 200 MB/s
Z	Several TB/s	< 200 GB/s

The CEPC online framework is divided into:
- ☐ Two levels of nodes:
- ☐ The buffer that link them.

- **First-Level Process Nodes**:
Event building and fast Reconstruction.
- **Second-Level Process Nodes**:
Full Reconstruction.
- **Buffer**:
1.Buffer data for calibration.
2.Isolate software on different level nodes.

As an online computing framework, RadarV3.0 will be implemented on level1 and level2 nodes.

CEPC TDAQ System Architecture

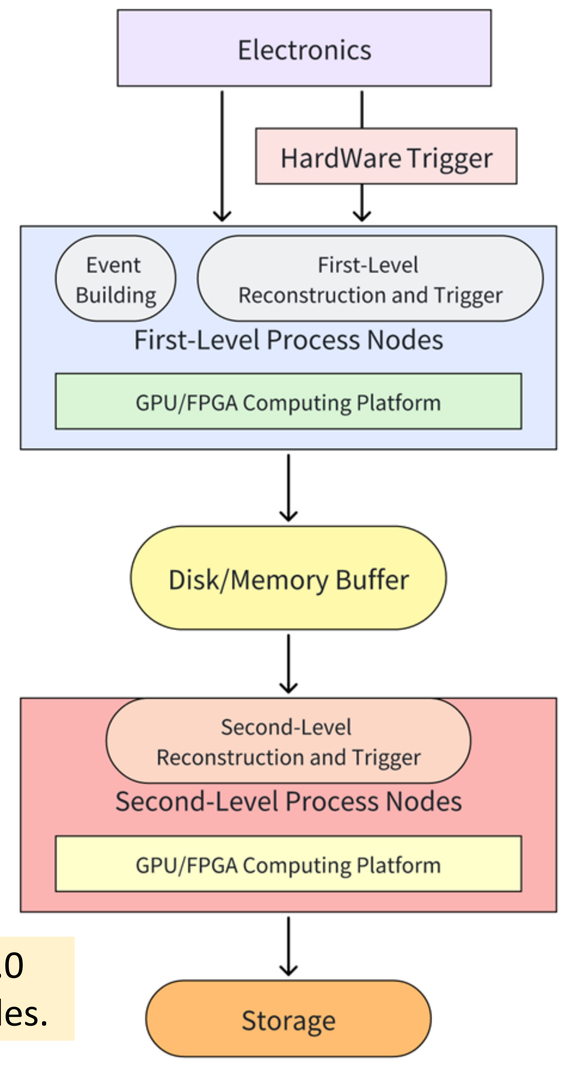

5.Conculusion

- For CEPC TDAQ, RadarV2.0 has the prospect of optimization.
- We are conducting research on heterogeneous computing and developing a high throughput and high bandwidth online heterogeneous computing framework RadarV3.0 for CEPC.

Development of the Aluminum stabilized superconductor for CEPC

中国科学院高能物理研究所
Institute of High Energy Physics
Chinese Academy of Sciences

Zhao Ling[12], Wang Menglin[12], Ning Feipeng[12], XU Qingjin[12], Hou Zhilong[12], Zhao yu[3], Liao hean[3],*

1 Institute of High Energy Physics, Beijing, China
2 University of Chinese Academy of Sciences, Beijing, China
3 Wuxi Toly Electric Works Co.,Ltd

Poster ID: 56
*C.A.: Ling Zhao
M.P.: +86-13661388942
Fax: +86-10-88236261
Email：zhaoling@ihep.ac.cn

Introduction

The Circular Electron Positron Collider （CEPC), to be hosted in China in a circular underground tunnel of approximately 100 km in circumference. A 3 Tesla superconducting solenoid magnet with cold bore of 7.07m serves as a key component of the large electron collider, providing a uniform and stable magnetic field for the detector.

Al-stabilized NbTi cable is and has been the universal choice until now for the detector magnets. Considering the large diameter of the coil and the 3 Tesla magnetic field, the conductor must satisfy simultaneously mechanical and industrial feasibility requirement. Two of all possible configurations have been studied in the CEPC R&D project.

Cold Mass Design

The main magnetic and geometrical design parameters of the cold mass are given respectively in table I. The cold mass has an overall thickness of 307mm. It consists of 276mm thick superconducting winding surrounded by a 30mm thick cylider.

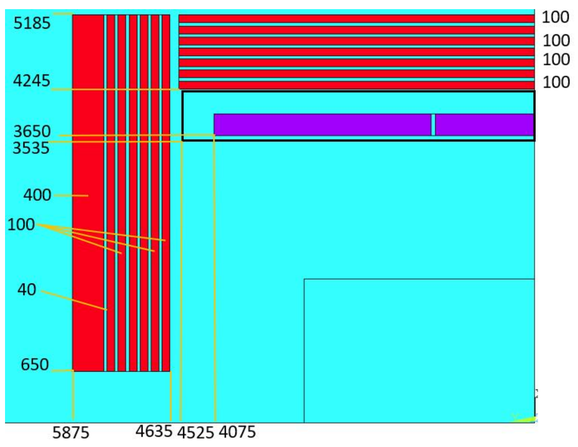

Geometrical design of the Magnet

Central magnetic field	3 T
Inner diameter	7.3m
Operating current	17000 A
conductor peak magnetic field	3.47T
Inductance	11 H
Stored Energy	1.54 GJ
Total number of turns	1400
Total cable length	33km

Conductor Design

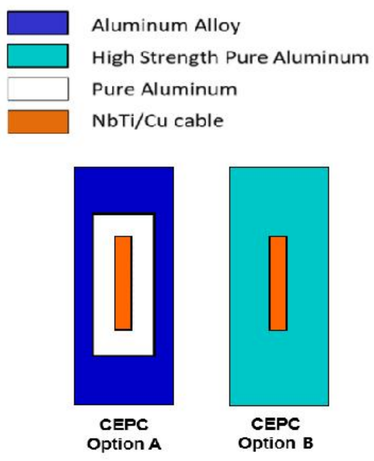

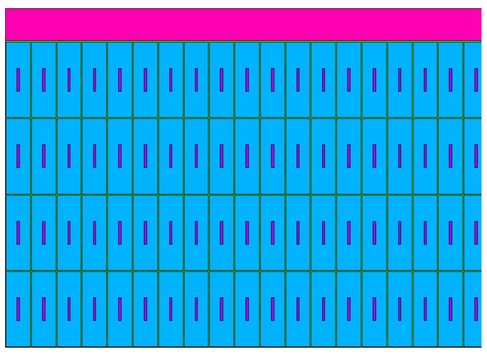

view of the winding

Material	Von Mises stress, MPa
Coil at 4.2 K	
Pure Aluminum	11.2-44
SC cable	180-234
Al alloy Support	34.3-57.2
Coil at 4.2 K, energized	
Pure Aluminum	40.3-46.2
SC cable	49.4-184
Al alloy Support	57.1-117

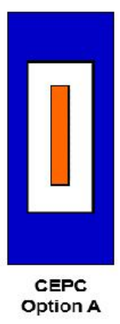

56mm*22mm

Material	Von Mises stress, MPa
Coil at 4.2 K	
Pure Aluminum	4.4-86.1
SC cable	174-243
Al alloy Support	4.6-36.2
Coil at 4.2 K, energized	
Pure Aluminum	41.5-95.9
SC cable	54.9-221
Al alloy Support	43.2-87.4

Maximum Von Mises stress in conductor's components

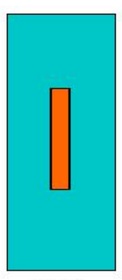

68mm*22mm

R&D of Box configuration conductor

Box configuration superconductor is obtained through a secondary co-extrusion process on the outside of aluminum-stabilized superconducting cable.

Al-stabilized cable

Dummy cable
56*22mm
Aluminium alloy+ copper4.7mm*15mm

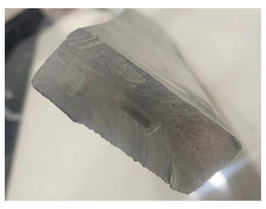

Box superconductor
56*22mm
Electrical grade Aluminium +4.7*15mm cable

- **Achieved the box configuration superconductor** from the electrical grade aluminum and 4.7mm*15mm cable **by a second coextrusion process**.
- Next, many attempts have been made by 6061 Alloy+10mm*33mm cable , but all failed because Aluminum Alloy need more higher temperature.

- Rutherfod cable:
  32 strands of NbTi
  pitch: 129mm
  fill factor: 86%
  Ic decay after stranding: <5%
- First extrusion:
  10mm*33mm(good)
- Second extrusion:
  22mm*56mm(failed)

Rutherford cable 32 strands

first co-extrusion pure Aluminum +Rutherford cable10*33mm

second co-extrusion 6061Alloy+cable(failed)

R&D of High Strength and High RRR Aluminum- Stabilizer

Yield strength > 100 MPa@4.2K, 74 MPa at room temperature, RRR value > 400

- By doping Ni-0.025% Be-0.025.
- The Al-0.025%Ni-0.025%Be alloy prepared from 4N8-aluminum achieved high 0.2% yield strength of 75MPa (R.T.) with RRR of 417.

Poisson's ratio	0.33/0.34
Young modulus	See the curve
Thermal expansivity	14.23×10^{-6} K^{-1}
$4.2KRp_{0.25}$	105MPa

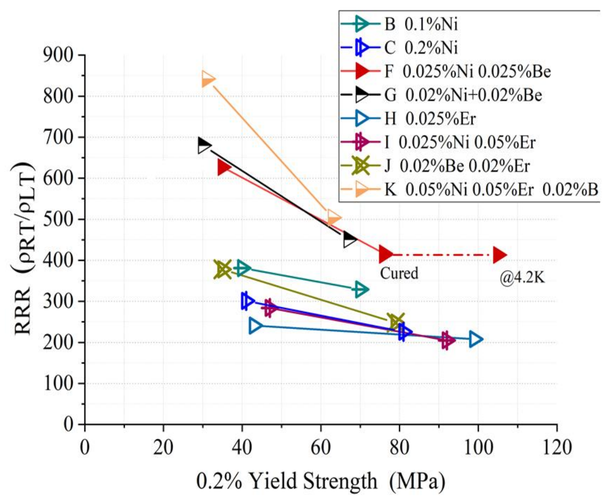

Progress of Al-Ni-Be Stabilizerd conductor

Rutherford cable 32 strands

The 32 strands Rutherford cable is inclosed inside the Al-Ni-Be alloy through a coextrusion process, and the size after that is 56*22mm. The critical current of strands e before and after coextrusion process was measured, and the measurement results are shown in the figure as below.

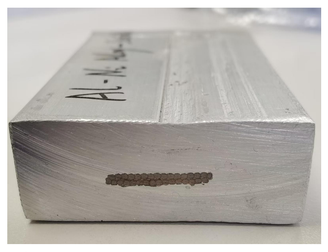

first co-extrusion Al-Ni-Be stabilizer +Rutherford cable 56mm*22mm

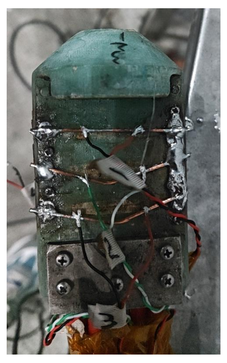

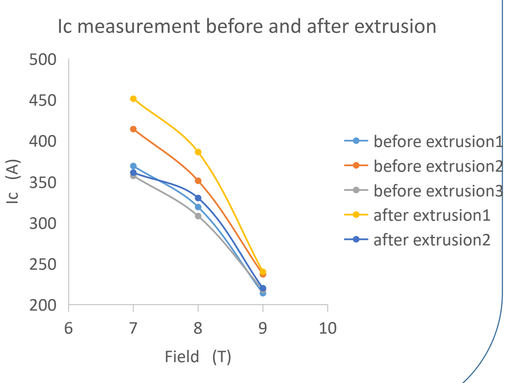

Conclusions

The stranding process for Rutherford cables and the coextrusion process for aluminum-stabilized superconductor have been established. The feasibility of the secondary coextrusion process has been verified using electrical grade Aluminum. However, the secondary coextrusion process based on aluminum alloy has not been get a good result. So Al-Ni-Be Stabilizerd conductor would be our choice for the ref-TDR.

Conceptual Mechanical Design and Analysis of CEPC Detector Magnet

Hou Zhilong, Ling Zhao, Feipeng Ning and Menglin Wang*
Accelerator Division, Institute of High Energy Physics, Beijing 100049, China
University of Chinese Academy of Sciences, Beijing 100049, China

中国科学院高能物理研究所
Institute of High Energy Physics
Chinese Academy of Sciences

*C.A.: Hou Zhilong
M.P.: +86-18600285402
Fax: +86-10-88236261
houzl@ihep.ac.cn

Abstract

A large-scale low-temperature superconducting magnet is proposed for the future detector of Circular Electron Positron Collider (CEPC) at the Institute of High Energy Physics, Chinese Academy of Sciences (IHEP,CAS). The central magnetic field of the magnet is 3 Tesla, the length, inner and outer diameter of the magnet is 9.05 m, 7.07 m and 8.47 m，respectively. The weight of the cold mass is about 185 t. This poster presents the mechanical design of the support structure of the cold mass and the cryostat of the magnet.

Introduction

The Circular Electron Positron Collider （CEPC）is a large scientific project proposed by the Institute of High Energy Physics, Chinese Academy of Sciences (IHEP,CAS) in China. The detector of the CEPC needs a 3 Tesla central magnetic field superconducting solenoid. The coil of the magnet is supported by an aluminum alloy cylinder and cooled indirectly by liquid helium to an operating temperature of 4.5K. Aluminum stabilized NbTi/Cu Rutherford cable is choosed to wind the coil. A room temperature bore is required with 7.07 m in diameter and 9.05 m in length. This poster presents the mechanical design of the magnet.

3D Structure Design

The mechanical structure of the detector magnet consists of vacuum tank, thermal shield, cold mass support. Figure 1. shows the structure of the magnet. Figure 2. shows the internal detailed structure of the magnet. Some parameters of the detector magnet are listed in Table 1. The vacuum tank, made of stainless steel, is installed in the barrel yoke. It houses and supports the superconducting coil.

Two chimneys are situated near the top of the vessel. Their purpose is the following:

i) the smaller chimney contains the cryogenic lines, maintaining the solenoid below 5 K during operation,

ii) the bigger one, contains the electrical leads, and is also used as the main pumping and venting line.

The thermal shield, made of 5083 aluminum, encloses the superconducting coil inside the vacuum tank.

The coil is suspended in the vacuum tank by titanium alloy rod. In order to ensure that the magnet operates stably, the heat leakage should be minimized.

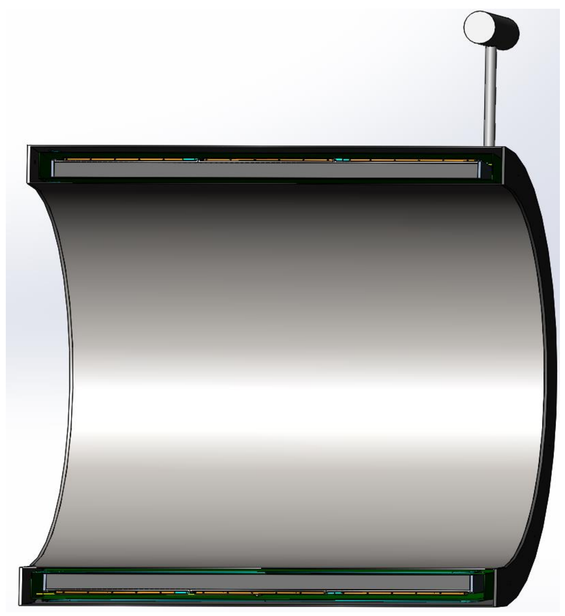

Fig. 1. Structure of the detector magnet

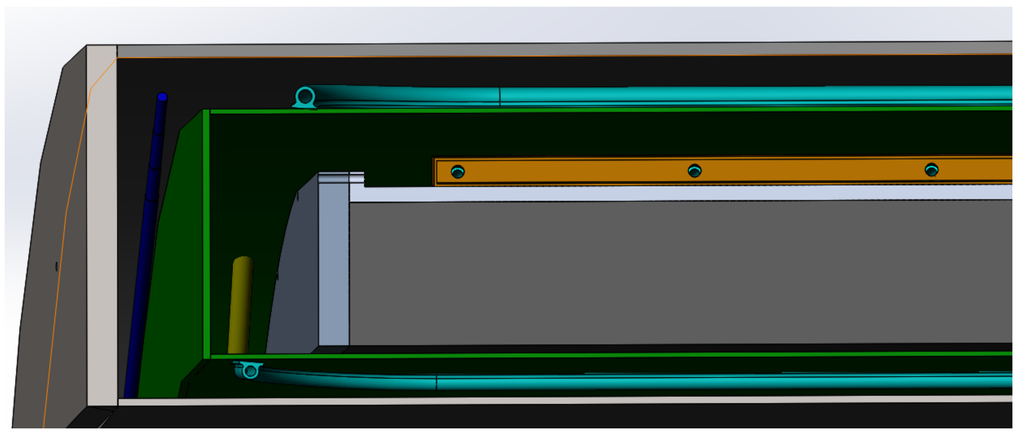

Fig. 2. Internal detailed structure of the detector magnet

Table 1. Parameters of the detector magnet

	Inner Diameter (mm)	Outer Diameter (mm)	Length (mm)
Vacuum tank	7070	8470	9050
Coil	7300	7916	8150

Suspending structure of coil

The coil suspend system has to ensure a precise and stable suspension of the cold mass inside the vacuum tank. The loads are the self-weight of the cold mass，the magnetic forces due to the decentering of misalignment of the coil with respect to the return yoke. The suspend system consists of a set of rods made of titanium alloy There are a total of 28 radial and axial rods, half at each end. Figure 3. shows the layout of the rods and the cold mass. Table 2. lists the parameters of the titanium alloy rods.

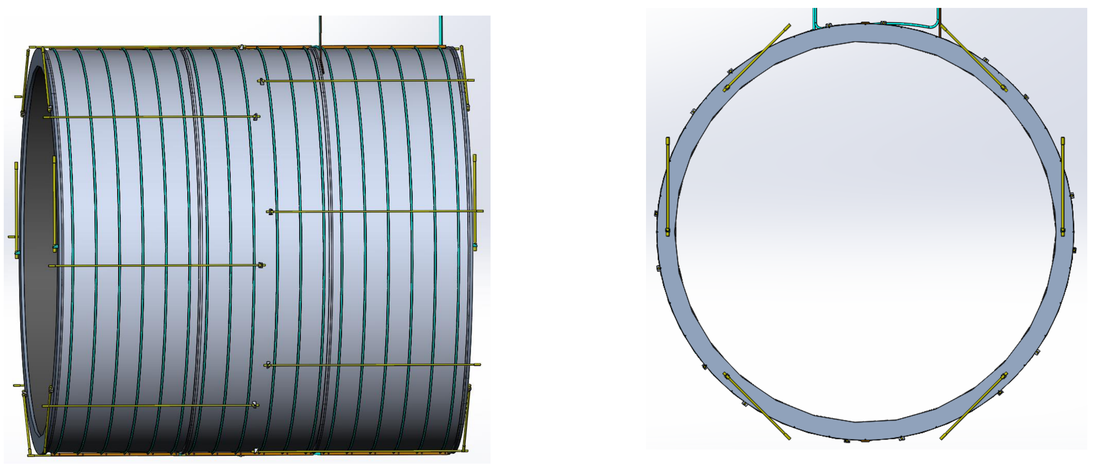

Fig. 3. Layout of the rods and the cold mass

Table 2. Parameters of the titanium alloy rods

Item	Diameter (mm)	Length (mm)	amount	Screw
Axial rods	30	3530	16	M36×3
Radial rods	40	1700	8	M48×4
Main pull rods	48	1650	4	M56×4

Vacuum tank Structure Analysis

The vacuum tank consists of two concentric cylindrical shells connected through structural welds by two end flanges. It must resist the huge electromagnetic force caused by cylindricity error and the decentering of misalignment of the solenoid when the magnet is excited, with respect to the return yoke, the pressure difference between inside and outside of the vacuum tank after vacuumed and the weight of the cold mass of the magnet. The calculation takes into account a 1.5 g acceleration in x and z direction(axial direction) and 2.5 g acceleration in y direction in the course of moving the magnet. Table 3. lists the electromagnetic force caused by misalignment.

According to the design guide of the cryogenic pressure vessel, the buckling stability and the mechanical strength is analyzed by using theoretical calculation and FEA. The thickness of the inner cylindrical shell is 15mm， the outer one is 25mm, and the end flanges is 60 mm. Figure 4. and figure 5. shows the deformation and stress distribution of the vacuum tank under maximum load and vacuum pressure.

Table 3. Induced loads of misalignment of solenoid

Misalignment of solenoid	Z(X,Y) 1 cm Rotation 0.14 rad	Z(X,Y) 3 cm Rotation 0.42 rad	Z(X,Y) 10 cm Rotation 0.14 rad
Displacement in Z direction （kN）	484	1498	5034
Displacement in X(Y) direction（kN）	34.3	236	656
Rotation around X Torque（kN•m）	1965	6170	19935

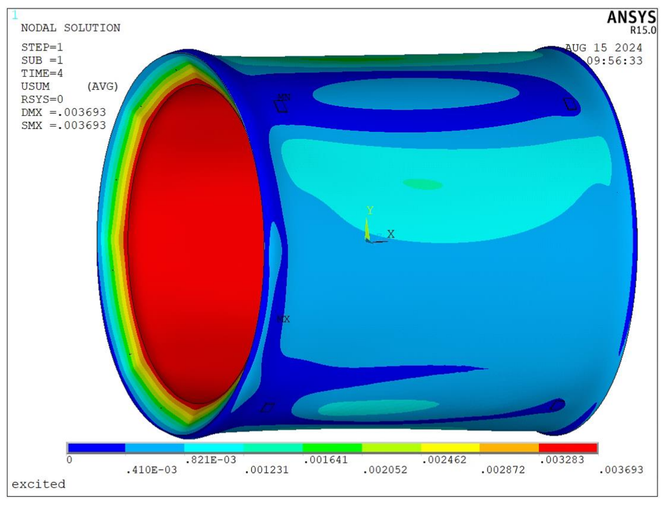

Usum $_{max}$=3.69 mm

Fig.4. Deformation distribution of vacuum tank.

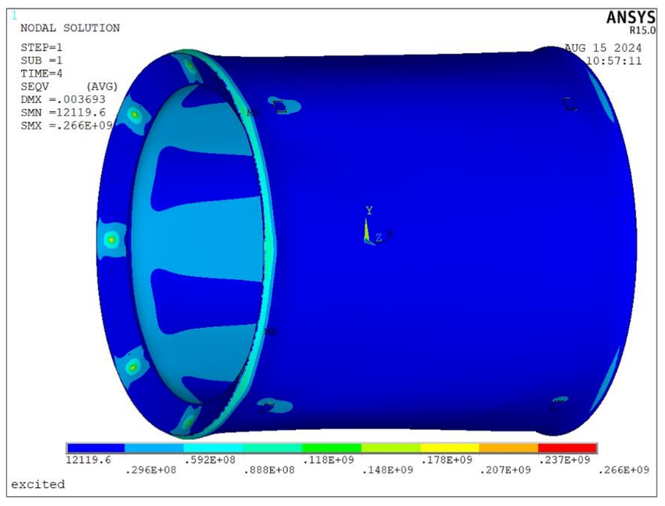

Seqv $_{max}$= 266 MPa

Fig.5. Stress distribution of vacuum tank.

Conclusions

The results of 3D structure analysis show that the maximum stress on the vacuum tank is 266 MPa, when the inner and outer cylindrical shells is 15 mm and 25 mm, respectively. The maximum stress is larger than the allowable stress of stainless steel. There are stress concentration points at the eight fixed positions. Nest step more fixed positions shall be added.

Poster ID:66 The 2024 International Workshop on the High Energy Circular Electron Positron Collider
2024/10/23 – 2024/10/27 – Hangzhou, China

Artificial Intelligence Applied Researches on Online Monitoring

Shuihan Zhang[1,2], Xiaolu Ji[1], Wenxi Pei [1,2], Huangteng Hu [1,2], Fei Li[1] , Kejun Zhu [1,2]

(1) State Key Laboratory of Particle Detection and Electronics, Institute of High Energy Physics, CAS, Beijing 100049, China
(2) University of Chinese Academy of Sciences, Beijing 100049, China

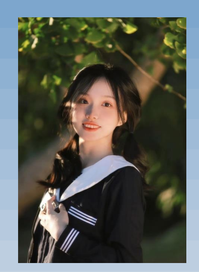

Introduction

The online monitoring system is an essential component of the data acquisition system, delivering swift, efficient, and comprehensive real-time monitoring for the readout chain. However, traditional online monitoring systems primarily rely on preset rules for data selection and inspection, which are unable to cope with complex operating conditions and large data volumes in real time. There are also problems that rely on manual monitoring and inspection, which is prone to omissions and inefficiency. This limitation makes it difficult for monitoring systems to accurately predict abnormal situations, severely impacting production efficiency and equipment safety. To address these challenges, the application of artificial intelligence technology has become a choice. A solution that **combines machine learning and large language model technology** for application on online monitoring systems has been designed to enhance the accuracy and efficiency of data inspection.

Requirements

Real-time, accurate, and comprehensive dynamic data quality monitoring

- Real-time feedback
- Promptly detect anomalies
- Improve data taking efficiency

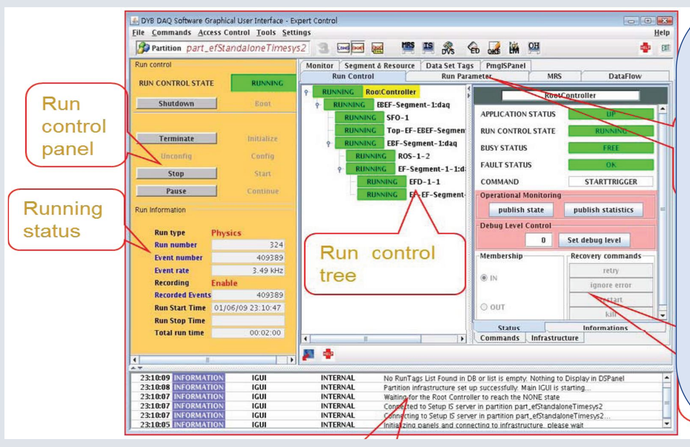

▶ **Monitoring Parameters**

- Real-time data quality monitoring
- Throughput & Rate
- System running status
- System resource utilization

Method Research

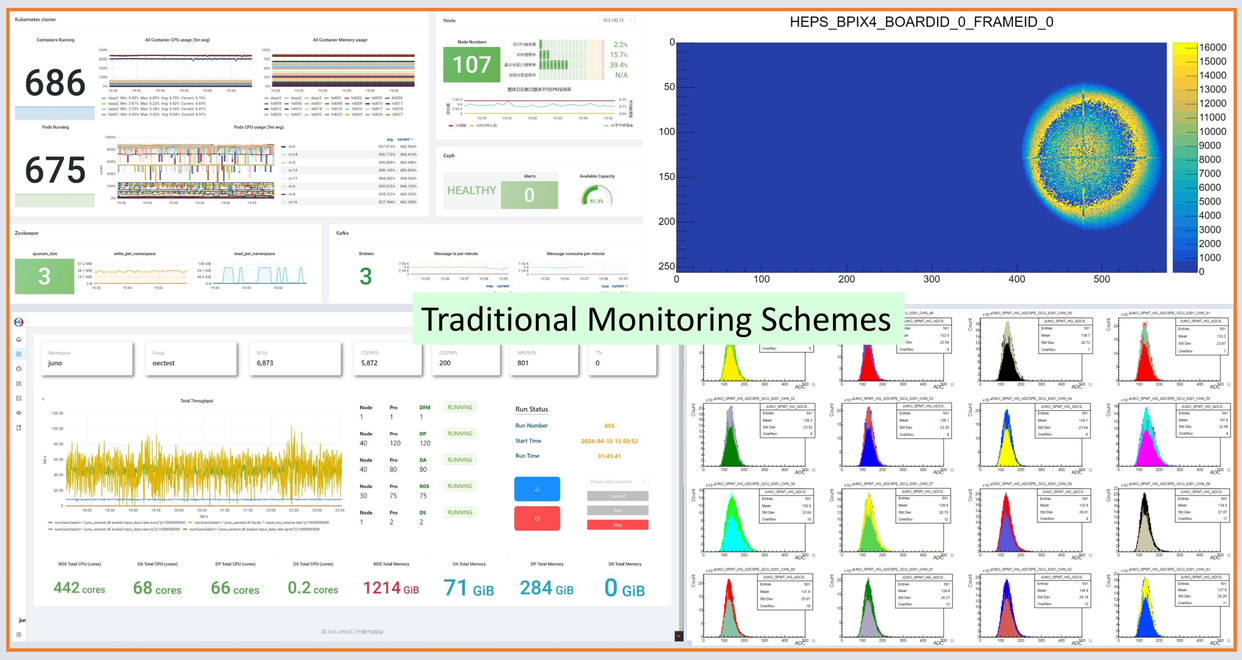

Traditional monitoring method:

- Calculate various physical parameters
- Compare with reference values
- Using preset rules to trigger alert mechanisms

AI-based monitoring method: Deploy different deep Learning models to automatically provide real-time intelligent recommendations and analyses

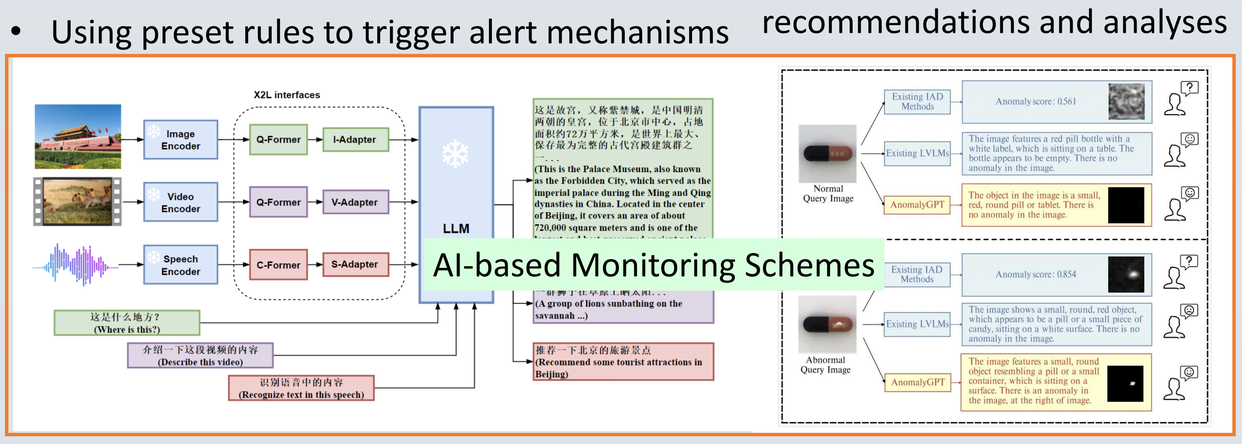

Aspect	Traditional Methods	AI-Based Methods
Data Analysis	Basic statistical methods	Machine learning for complex patterns
Response Mechanism	Human intervention required	Automated and faster responses

Current Research Progress

▶ **Intelligent interaction**

Motivation: Intelligent Q&A system, assisting with shifts

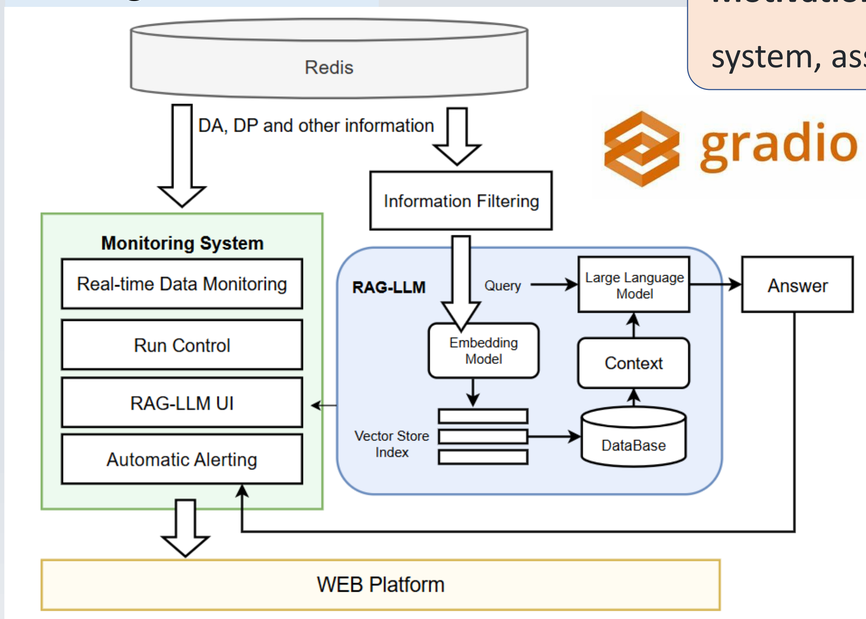

Establishing a local knowledge base → Expanding proprietary domain knowledge → Deploying local models → Prompt

RAG: Document precise retrieval, reduce illusion answers

LLM: Question and Answer

▶ **Automated anomaly detection**

Model Training: nearly 200,000 samples

Model Optimization: parameter evaluation & structural optimization

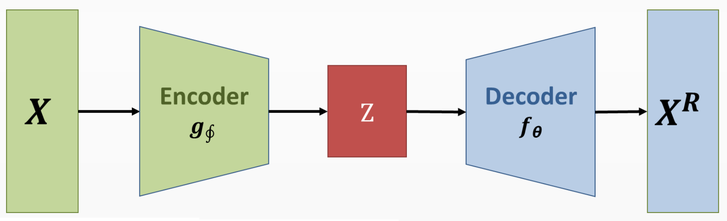

Motivation: Real-time detect anomaly, reduce manual workload

CPU	Number of images	Detection time	Precision
AE model	2560	0.2324s	0.64
statistical methods	2560	2.3433s	0.33

▶ **Current results**

- Reduced manual workload by 60%
- Predicted 99% of the anomaly data

Future Work

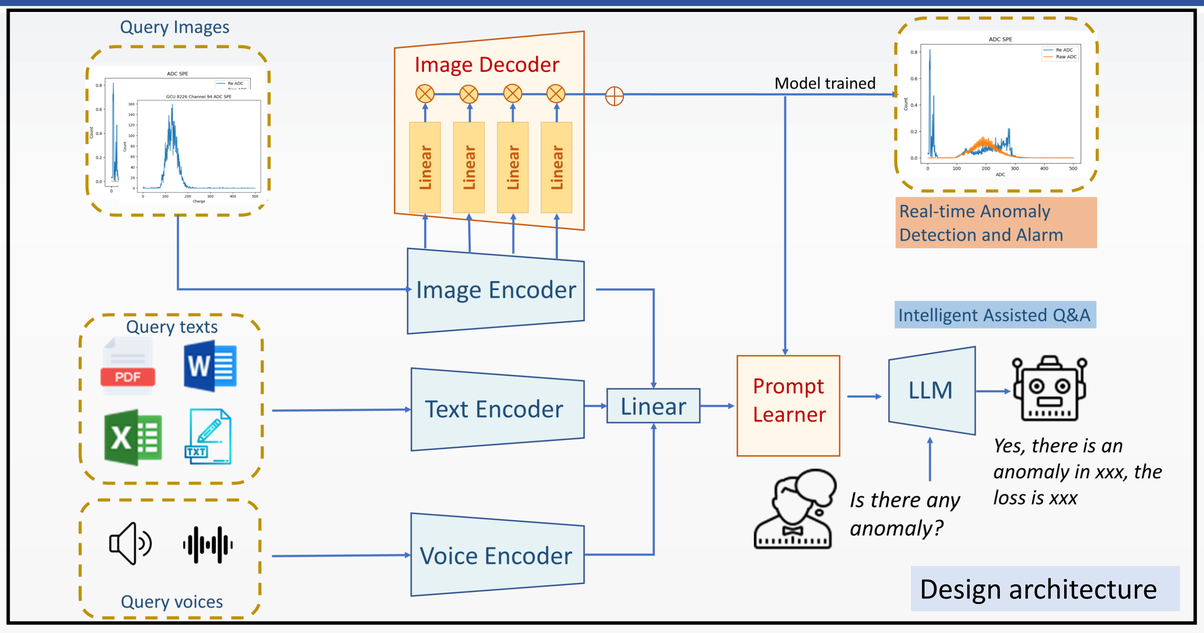

▸ **Enhanced Natural Language Processing Capabilities**: Multilingual support & Contextual understanding & Automated report generation

▸ **Intelligent Anomaly Detection and Prediction**: Multisource data fusion

▸ **Human-Machine Collaboration and Interaction:** Interactive interfaces and assistants & Feedback loop

▸ **In the future, AI technology will provide more options for efficient design solutions**

Poster ID: 72

Studies on timing performance of BGO crystal scintillator

Zhiyu Zhao[3,4,5], Baohua Qi[1,2], Dejing Du[1,2], Fangyi Guo[1,2], Jiyuan Chen[4,5,3], Yong Liu[1,2]

1. Institute of High Energy Physics, Chinese Academy of Sciences, 19B Yuquan Road, Beijing, 100049, China
2. University of Chinese Academy of Sciences , 19A Yuquan Road, Beijing, 100049, China
3. Tsung-Dao Lee Institute, Shanghai Jiao Tong University, 1 Lisuo Road, Shanghai 201210, China
4. Institute of Nuclear and Particle Physics, School of Physics and Astronomy, 800 Dongchuan Road, Shanghai 200240, China
5. Key Laboratory for Particle Astrophysics and Cosmology (MOE), Shanghai Key Laboratory for Particle Physics and Cosmology (SKLPPC), Shanghai Jiao Tong University, 800 Dongchuan Road, Shanghai 200240, China

Introduction

The future Circular Electron-Positron Collider (CEPC) is envisioned as a large-scale Higgs factory. For its detector system, a highly granular crystal electromagnetic calorimeter has been proposed to deliver 5D information, encompassing the x, y, z coordinates, energy (E), and time (t). This calorimeter features a homogeneous structure with long crystal scintillator bars as the active material, with BGO crystals and SiPMs identified as the preferred components. The role of time information in calorimeters is increasingly critical; it not only helps distinguish pile-up effects but also aids in particle identification, shower reconstruction, and enhances the calorimeter's energy resolution. Therefore, optimizing and understanding the timing performance of this detector design is of paramount importance. The timing resolution of the detector unit, consisting of a BGO crystal and two SiPMs, was thoroughly studied through beam tests and simulations under various conditions.

Timing Methods

- Setup of a cosmic ray experiment

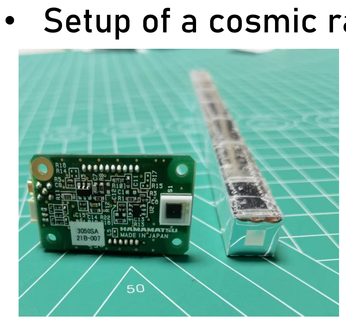

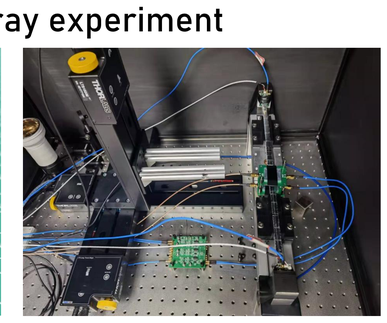

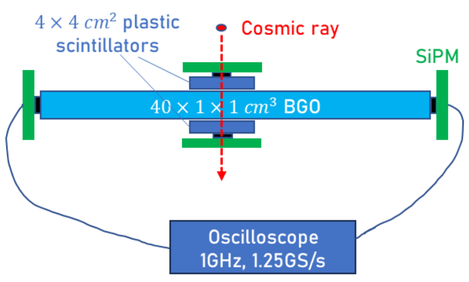

- Comparison of three timing methods

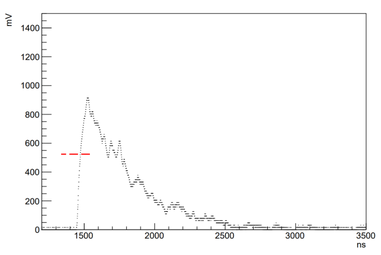

a. Constant fraction

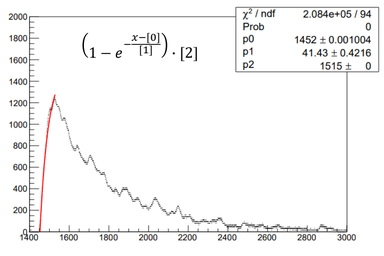

b. Leading edge fitting

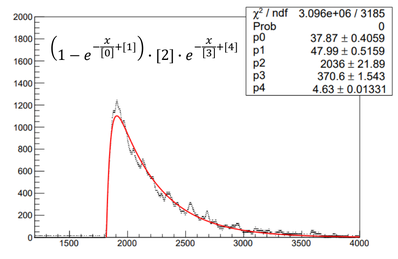

c. Waveform fitting

- The method of leading edge fitting gives the best time resolution result.
- Time resolution depends on the fraction. Stochastic fluctuation of photon's arrival time increase as the fraction, while the noise decreases with increasing threshold.

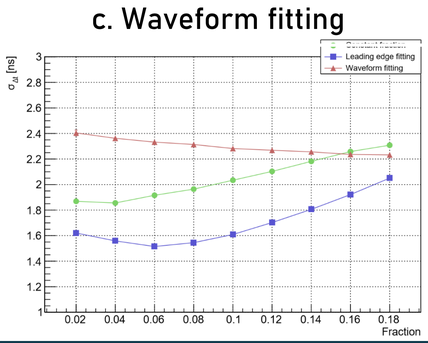

Time resolution - MIP

- CERN PS T9, 10GeV pion beam, 26 Jun. ~ 10 Jul. 2024
- The time resolution of BGO with lengths ranging from 4 to 40 cm is from 0.45 to 0.75 ns, and it worsens with increasing doping concentration. For PWO crystals, with lengths ranging from 2 to 16 cm, the time resolution is between 0.2 and 0.375 ns, which is better than that of BGO.

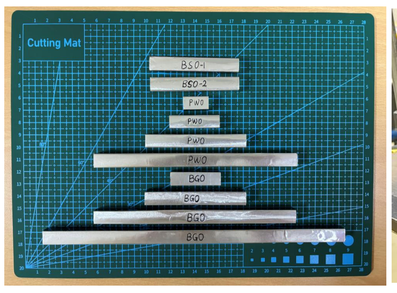

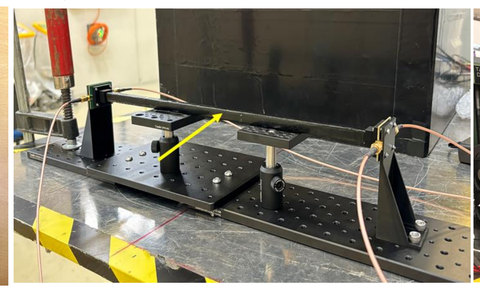

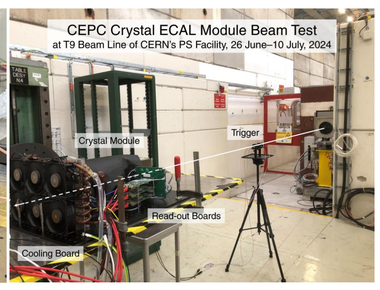

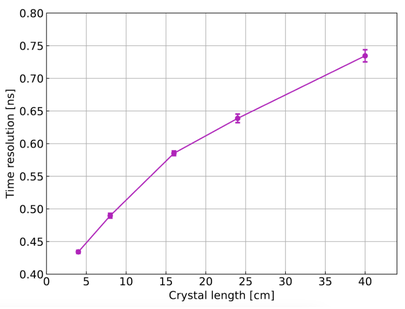

a. Results of 4~40cm BGO bars. The time resolution improves as the crystal length decreases.

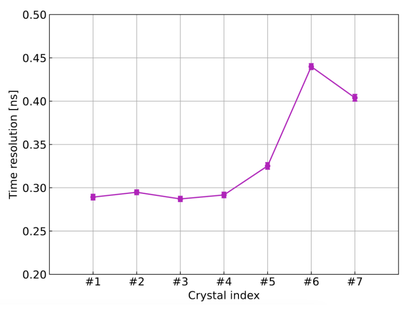

b. 2cm BGO with different doping concentrations (100ppm, 200ppm, 500ppm, 1000ppm, 2000ppm, 5000ppm, 5000ppm)

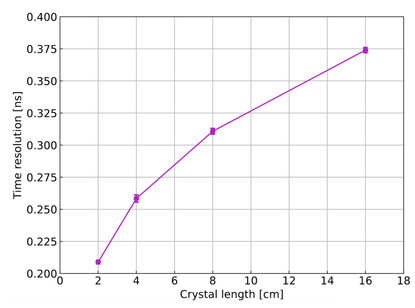

c. Results of 2~16cm PWO. The time resolution of PWO is better than that of BGO with the same length, dominated by decay time.

Simulation

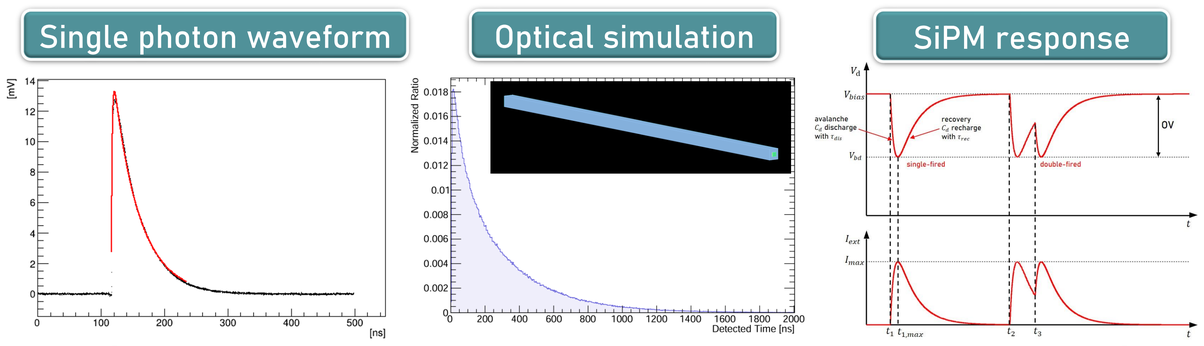

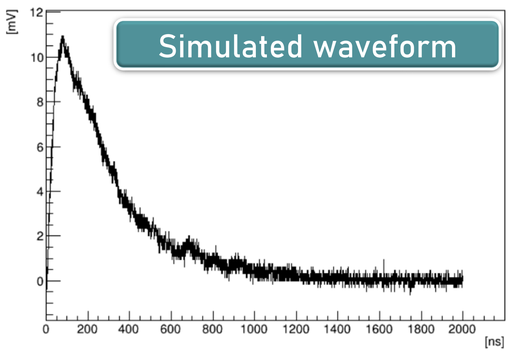

- Track the time, wavelength and other information of each detected photon in Geant4. Then, combine the measured single-photon waveform and SiPM response principle to superimpose and obtain the final waveform.

- Adjustable parameters:
  - Crystal: type, geometry, optical properties
  - SiPM: pixel density, PDE, recovery time, waveform
  - DAQ: sampling rate, vertical accuracy, noise, amplification
- Light yield and scintillation decay time have the greatest impact on time resolution, while sampling rate and amplification factor have minimal effect on time resolution.

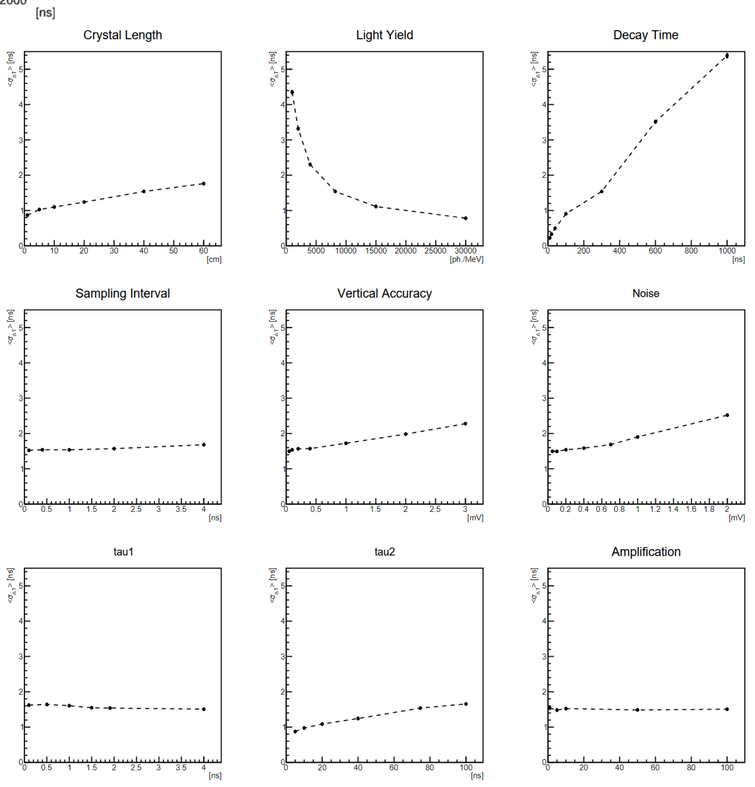

Time resolution - Electron

- DESY TB22, 1~5GeV electron beam, Oct. 2023

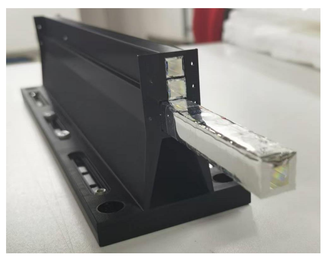

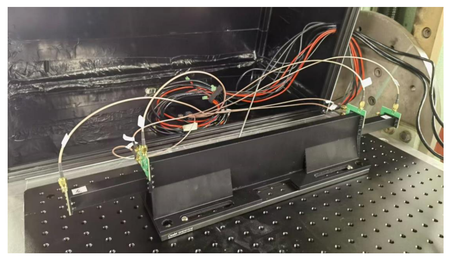

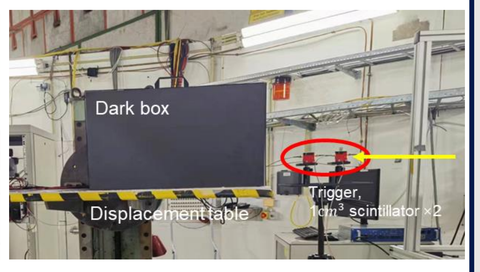

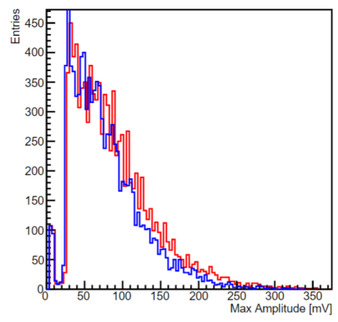

a. Signal Amplitude

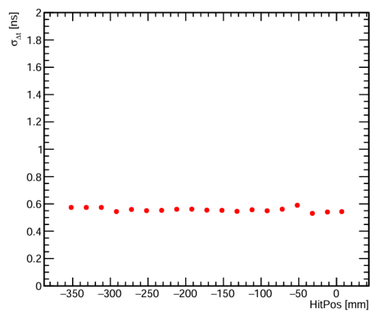

b. Time resolution scanning for 40cm BGO

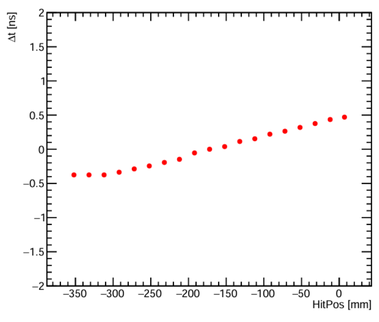

c. Time difference at various incident positions

- Additional crystals are placed in front of the tested crystal as a pre-shower to study the time resolution of EM showers at different depths.
- Time resolution at the shower maximum region is better than 200ps.

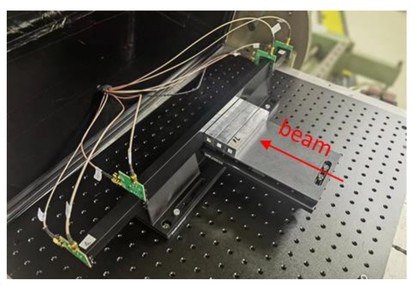

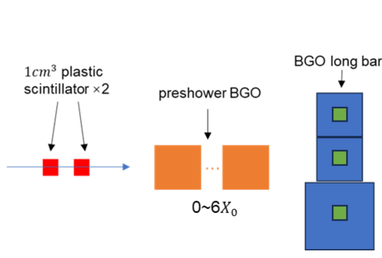

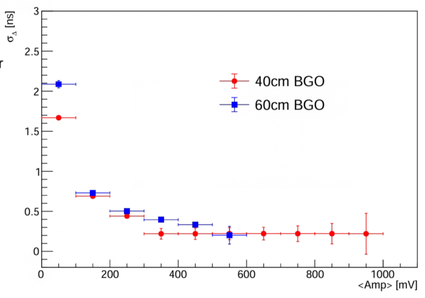

Summary

This study investigate the time resolution of the BGO-SiPM module, the basic unit of the highly granular crystal ECAL. Through comparative analysis, the leading-edge fitting method was identified as the optimal timing technique. Beam tests were conducted under various conditions, measuring the time resolution of BGO crystals (4 to 40cm) at 1-MIP using a pion beam, with results ranging from 0.45 to 0.75ns. An electron beam was also used to assess a 40/60cm BGO crystal at different shower depths, achieving an optimal resolution of 0.2 ns. Simulations were performed to identify key factors influencing time resolution, such as light yield and decay time.

Poster ID: 73

Studies on the dynamic range of SiPMs with high pixel densities

Zhiyu Zhao[3,4,5], Baohua Qi[1,2], Shu Li[3,4,5], Yong Liu[1,2]

1. Institute of High Energy Physics, Chinese Academy of Sciences, 19B Yuquan Road, Beijing, 100049, China
2. University of Chinese Academy of Sciences , 19A Yuquan Road, Beijing, 100049, China
3. Tsung-Dao Lee Institute, Shanghai Jiao Tong University, 1 Lisuo Road, Shanghai 201210, China
4. Institute of Nuclear and Particle Physics, School of Physics and Astronomy, 800 Dongchuan Road, Shanghai 200240, China
5. Key Laboratory for Particle Astrophysics and Cosmology (MOE), Shanghai Key Laboratory for Particle Physics and Cosmology (SKLPPC), Shanghai Jiao Tong University, 800 Dongchuan Road, Shanghai 200240, China

Energy dynamic range of CEPC Crystal ECAL

- The future Circular Electron-Positron Collider (CEPC) is envisioned as a large-scale Higgs factory. A highly granular crystal ECAL has been proposed to address major challenges in jet reconstruction and achieve optimal EM resolution of around 2–3%/$\sqrt{E}$ for CEPC. This calorimeter features a homogeneous structure with BGO long crystal bars as the active material, and SiPMs as optional photon sensors.

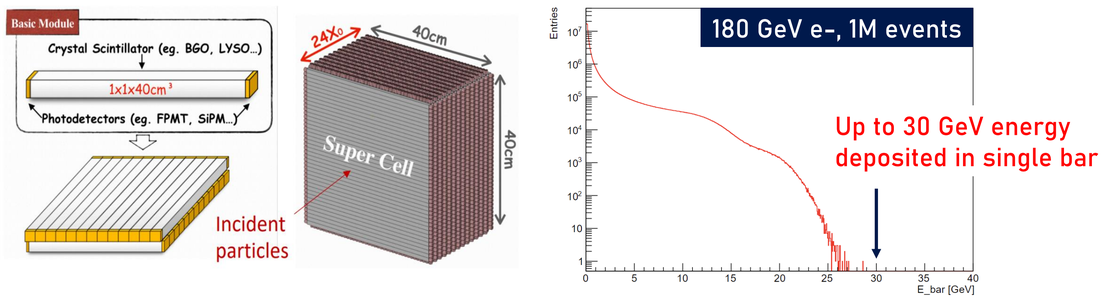

- At center-of-mass energies ranging from 240GeV to 360GeV, the energy deposition in a single crystal bar can reach up to 30GeV, potentially resulting in the detection of approximately 337k photoelectrons per channel. This places significant demands on the dynamic range of SiPMs.

Experiment setup

- An experiment using PMT operated at different gains as a scaler to measure the intrinsic dynamic range of SiPM with large pixel densities.

PMT – main scaler: by applying different bias voltages to operate at different gains, linear response is maintained across the entire input range

Pico-second laser – light source: 405nm wavelength with a pulse width of less than 40ps to prevent multiple firing of SiPM pixels

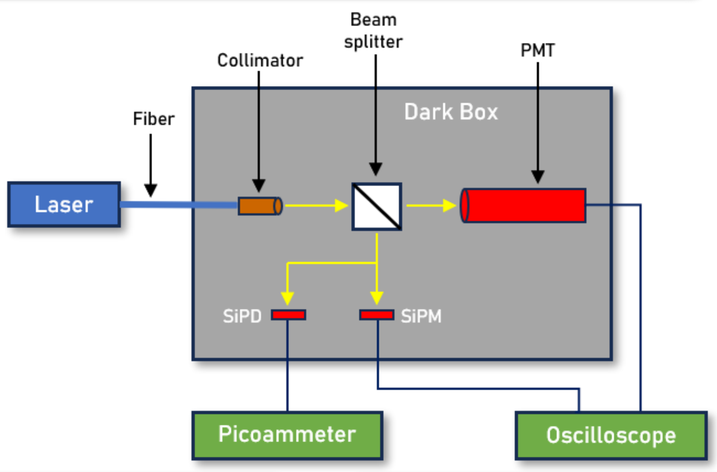

SiPD – auxiliary scaler: calibrated the laser intensity and selected the linear region for PMT

SiPM – DUT with different pixel densities

Scaler Calibration

- Selection on PMT's operation modes under different light intensities.

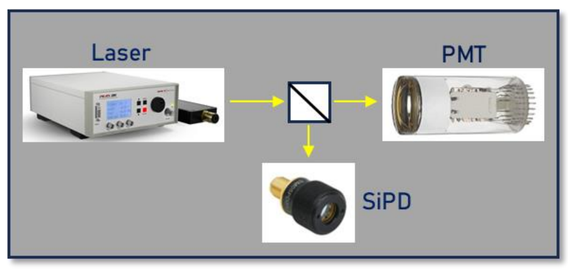

Response of PMT

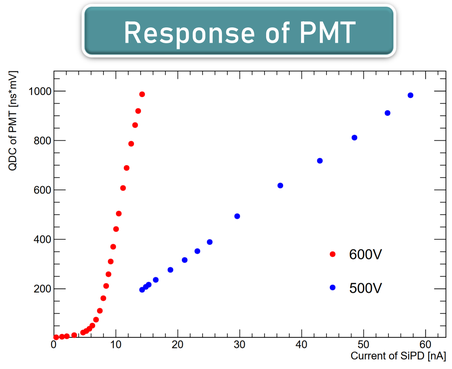

PMT gain calibration

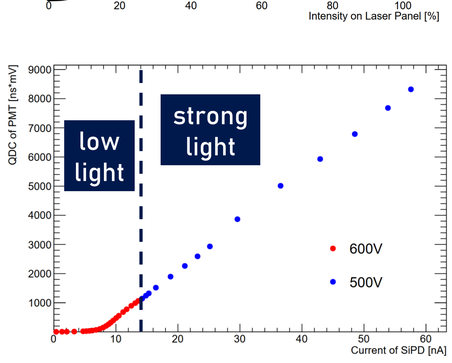

- After calibration, PMT can always keep a linear response within the whole input range. And the number of incident photons on SiPM can be evaluated by PMT's output.

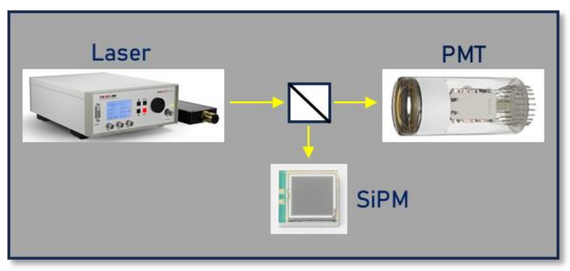

Responses of PMT and SiPM

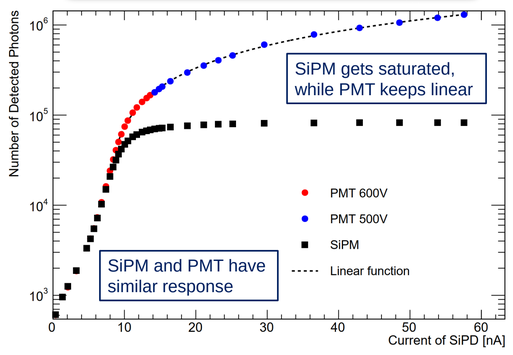

SiPM response to pico-second laser

SiPM	Pixel Pitch (μm)	Active Area (mm^2)	Nominal pixel counts	PDE (%) $\lambda = \lambda_p$
HPK S13360-6025PE	25	6.0×6.0	57600	25%
HPK S14160-3010PS	10	3.0×3.0	89984	18%
NDL EQR06 11-3030D-S	6	3.0×3.0	244719	30%

HPK S13160-6025PE | HPK S14160-3010PS | NDL EQR06 11-3030D-S

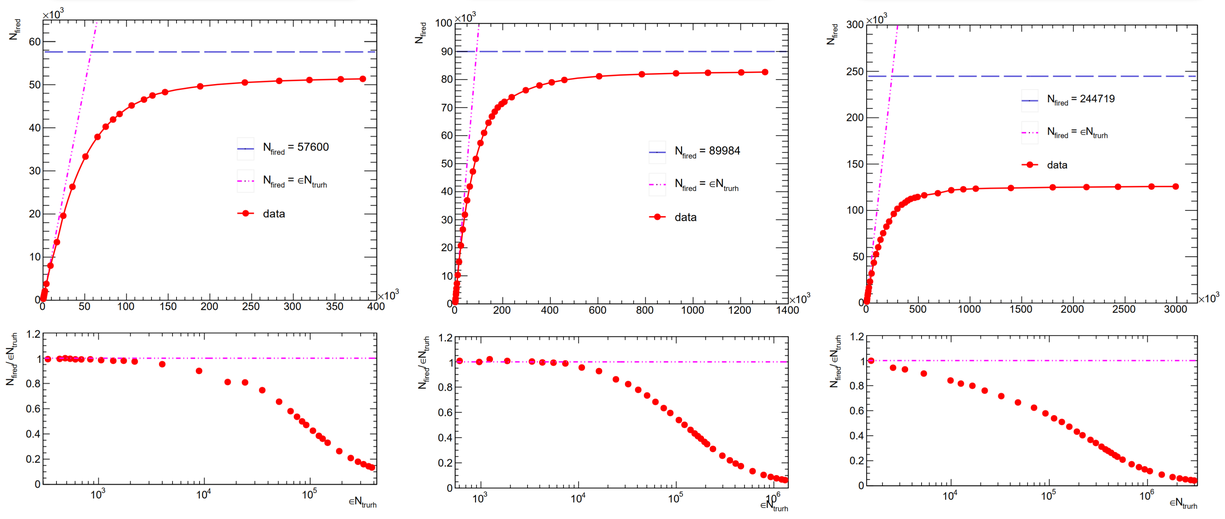

- Saturation values are close to but a little smaller than their pixels number.
- Non-linearity starts at very beginning region, and saturation value is only half of its pixel number. (Further researches are need for this type of SiPM)

SiPM	Nominal pixel counts	Max. photon counts	5% non-linearity
S13360-6025PE	57600	51347	4246
S14160-3010PS	89984	82664	11750
EQR06 11-3030D-S	244719	125775	2433

Simulation – SiPM response to BGO scintillation

- A Monte Carlo model to simulate the SiPM response to BGO($40 \times 1 \times 1 cm^3$) scintillation light. The model includes both BGO and SiPM properties.

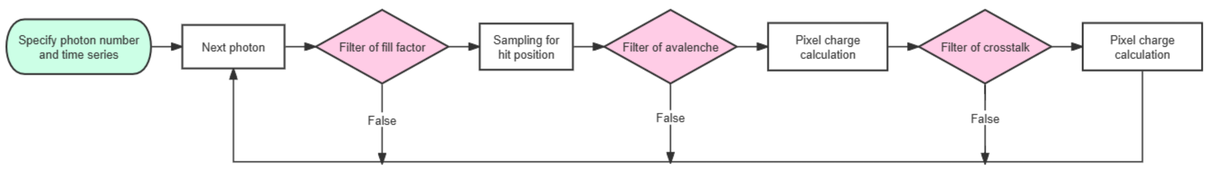

Single photon waveform | BGO optical simulation | SiPM response model

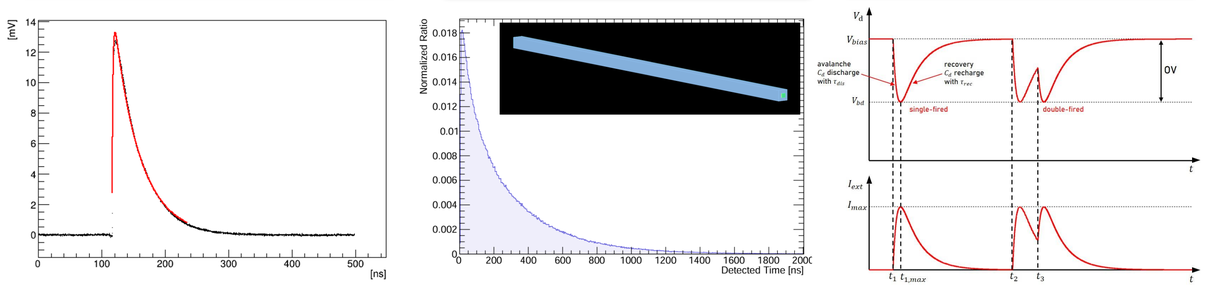

SiPM pixels can be fired multiple times due to the recovery effect

HPK S13160-6025PE | HPK S14160-3010PS | NDL EQR06 11-3030D-S

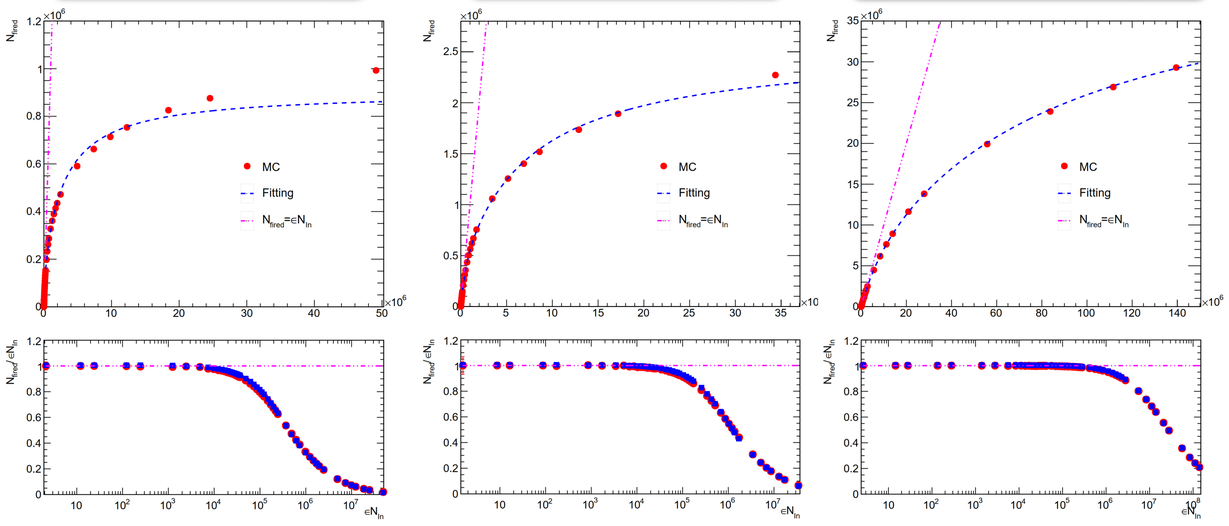

SiPM	Max. photon counts	5% non-linearity
HPK S13360-6025PE	57600	19592
HPK S14160-3010PS	89984	53747
NDL EQR06 11-3030D-S	244719	1106210

- The non-linear behaviors of SiPM are delayed due to the long decay time of BGO scintillation.
- SiPMs with 10μm pixels are potentially sufficient for CEPC crystal ECAL.

Summary

- Design an experiment to measure the intrinsic dynamic range of SiPMs with large pixel numbers under pico-second laser.
- Build a MC model for simulating the SiPM response to BGO scintillation. The simulation results show that SiPM with 10μm pixels can keep a linear response within the 30GeV (337k p.e. per channel) energy dynamic range.

Preliminary design consideration for CEPC fast luminosity feedback system

Meng Li[1,2], Philip Bambade[3], Dou Wang[1], Haoyu Shi[1], Jie Gao[1], Sha Bai[1]
[1]Institute of High Engergy Physics, Chinese Academy of Sciences; [2]University of Chinese Academy of Sciences;
[3]Laboratoire de Physique des 2 infinis Irène Joliot-Curie–IJCLab

Introduction

With very small beam sizes at IP (several tens of nanometers in the vertical direction) and the presence of strong FFS quadrupoles in the CEPC, the luminosity is very sensitive to the mechanical vibrations, requiring excellent control over the two colliding beams to ensure an optimum geometrical overlap between them and thereby maximize the luminosity. Fast luminosity measurements and an IP orbit feedback system are therefore essential. In this paper, we will show the preliminary design consideration for a fast luminosity feedback system at CEPC.

Orbit feedback methods

There are two methods for the IP orbit feedback system at CEPC[1,2,3]:

- **Beam-beam deflection driven method [vertical]**

  The small offset between the two colliding beams at IP can introduce an deflect angle due to beam-beam effect, which will be converted into a large offset as the beams propagate forward and collide, by measuring this beam orbit with BPMs around IP, can estimate the offset and sign at the IP.

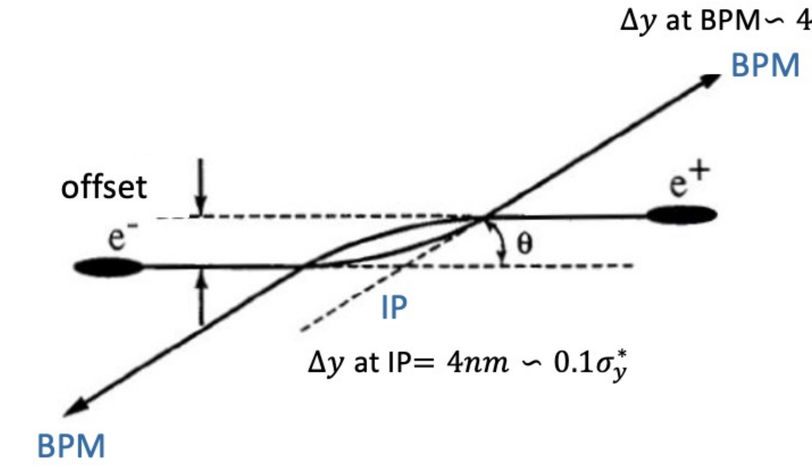

- **Luminosity driven system [horizontal]**

  Based on the measurement of the luminosity, we can know the offset between two beams, but cannot easily know its sign. And many other effects may also cause luminosity changes at relatively low frequency, should introduce a dithering with certain frequency.

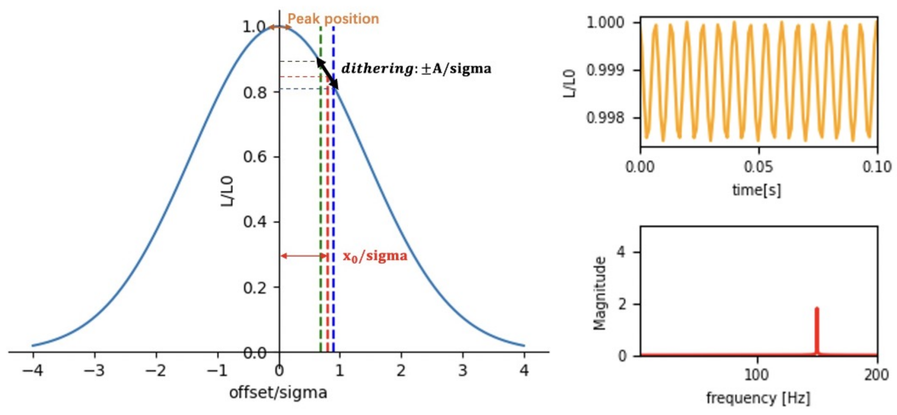

Vertical—Beam-beam deflection driven method

Using the beam-beam deflection method for vertical orbit feedback at the IP, our preliminary scheme is to place 2 paris of BPMs on both sides of the IP for each ring.

CEPC [Scheme]	β^*_x/β^*_y [m/mm]	σ^*_x/σ^*_y [μm/nm]	ξ^*_x/ξ^*_y	$\Delta x_{IP}/\Delta y_{IP}$ [μm/nm]	$\Delta x'/\Delta y'$ [μrad]	$\Delta x_{BPM}/\Delta y_{BPM}$ [μm]
Z	0.13/0.9	6/35	0.004/0.127	0.6/3.5	-0.1/-3.1	-0.1/-2.8
WW	0.21/1.0	13/42	0.012/0.113	1.3/4.2	-0.5/-3.0	-0.4/-2.7
Higgs	0.30/1.0	14/36	0.015/0.11	1.4/3.6	-0.4/-2.5	-0.4/-2.2
$t\bar{t}$	1.04/2.7	39/113	0.071/0.1	3.9/11.3	-1.7/-2.6	-1.4/-2.4

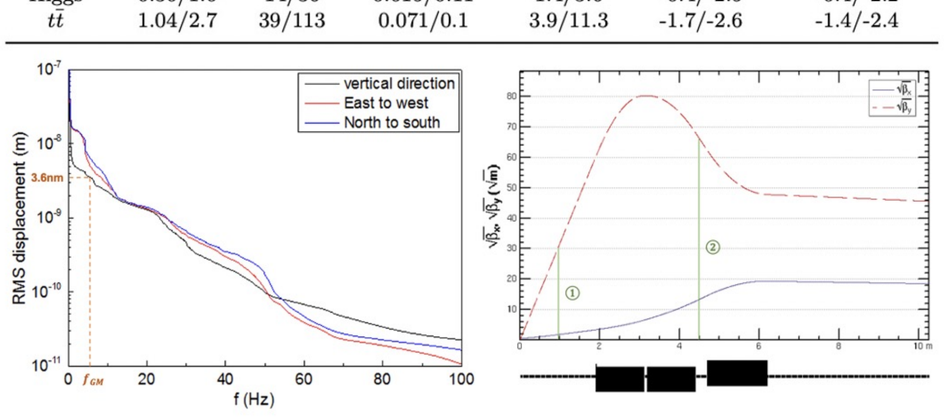

① The initial designed BPM ($0.2\mu m$@$500Hz$) → **good enough for vertical direction**

$$\Delta y_{BPM} = \sqrt{\beta^*\beta_{BPM}}\Delta y' \approx s * \Delta y' = 0.85\times(-2.5\mu rad) = 2.2um \approx 11\ \mathrm{BPM_{res}}@500\mathrm{Hz}$$

$$\Delta x_{BPM} = \sqrt{\beta^*\beta_{BPM}}\Delta x' \approx s * \Delta x' = 0.85\times(-0.4\mu rad) = 0.4um \approx 0.4\ \mathrm{BPM_{res}}@100\mathrm{Hz}$$

② Utilize 2 pairs of BPMs → **potential BPM failures or decreased accuracy and resolution**

→ add another pair of BPMs at locations with larger βy values ($\pm 4.5m\ far\ from\ IP$):

$$\Delta y_{BPM} = \sqrt{\beta^*\beta_{BPM}}\Delta y' \approx \sqrt{1\times10^{-3}}\times66\times(-2.5\mu rad) = 5.2um \approx 26\ \mathrm{BPM_{res}}@500\mathrm{Hz}$$

Horizontal—Fast Luminosity Monitor

The fast luminosity monitor based on radiative Bhabha at zero degree, which has a very large cross section ($\approx 150mbarn$). Find 3 possible detector positions where the loss rate is large enough and radiative Bhabha at zero degree process dominates over the sum of other particles loss processes.

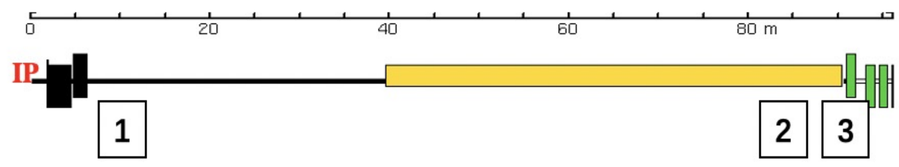

	Position1	Position2	Position3
Distance from IP	10m	84m	90.5m
Average Number detected/collision	3.4(two sides)	3(one side)	3.2(one side)
Average Number detected/ms	2830	2500	2670
Expected Measured Precision	1.9% @1kHz	2.0% @1kHz	1.9% @1kHz
Average Energy of scattered electron	24GeV	70GeV	75.3GeV
Average Hitting Angle	1.7×10^{-4}rad	7×10^{-4}rad	7×10^{-4}rad
Maximum Secondary Particle Position	88mm	104mm	105mm
Detection Area	$5\times20cm^2$	$3\times15cm^2$	$3\times15cm^2$
Backgrounds	SR Photons in 1 Side	-	-
Beam-Beam Deflection Impact	sensitive	less sensitive	less sensitive
Detector Number	2	1	1
Detector Measurement Parameters	Number of signals within 1ms		
Detector Time Resolution	600ns		
Detector technology possibility	LGAD, SiC, Diamond		

Conclusion

- **Fast Luminosity Tuning System, including fast BPMs and fast luminosity monitor, would be necessary for CEPC.We already have some candidate positions and potential detector solutions.The detailed design of the detectors is get started.**
- **More detailed simulations needs to be done to study more, including determine the detailed location and quantity of BPMs and the design of detectors and feedback.**

[1] Y. Funakoshi et al., “Interaction point orbit feedback system at SuperKEKB”, in Proc. 6th Int. Particle Accelerator Conf. (IPAC’15), Richmond, VA, USA, May 2015.
[2] D. El Khechen, “Fast Luminosity Monitoring Using Diamond Sensors for SuperKEKB”, PhD thesis, Université Paris-Sud, Orsay, France, 2016.
[3] C. G. Pang et al., "A fast luminosity monitor based on diamond detectors for the SuperKEKB collider", Nucl.Instrum.Meth. A931 (2019) 225-235.

Poster ID: 102

Status and Performance of LumiBelle2 in the 2024 Beam Operation of SuperKEKB

M. Li[1,2,3], P. Bambade[3], S. Wallon[3], H. Nakayama[4], S. Uehara[4]
[1]Institute of High Engergy Physics, Chinese Academy of Sciences; [2]University of Chinese Academy of Sciences;
[3]Laboratoire de Physique des 2 infinis Irène Joliot-Curie–IJCLab; [4]KEK, 305-0801 Tsukuba, Japan

Introduction

LumiBelle2 is a fast luminosity monitoring system designed to do fast luminosity feedback and machine tuning for SuperKEKB. It uses sCVD diamond detectors placed in both the electron and positron rings to measure the Bhabha scattering process at vanishing photon scattering angle. The system provides Train-Integrated-Luminosity signals at 1 kHz for dithering feedback and Bunch-Integrated-Luminosity signals at 1 Hz to monitor variations along the bunch trains. From July 2022 to the end of 2023, SuperKEKB had a long shutdown for maintenance and upgrades. In order to ensure LumiBelle2 satisfactory operation during the 2024ab run, a program of checks and calibrations of the LumiBelle2 hardware and software components was implemented before the restart of the accelerator complex. In this paper, the updated status of LumiBelle2 is reported followed by a report on obtained luminosity monitoring performance, based on the new data.

CURRENT SETUP

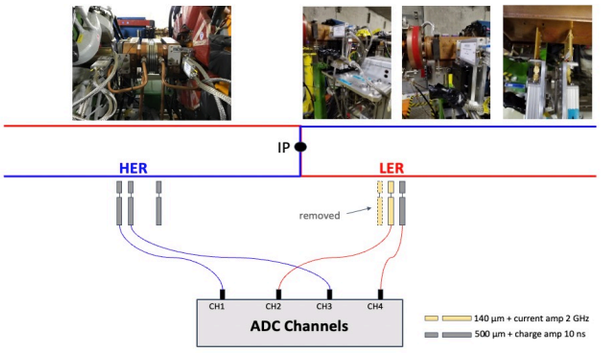

RESULTS IN 2024ab RUN

- **Train integrated luminosity signals**

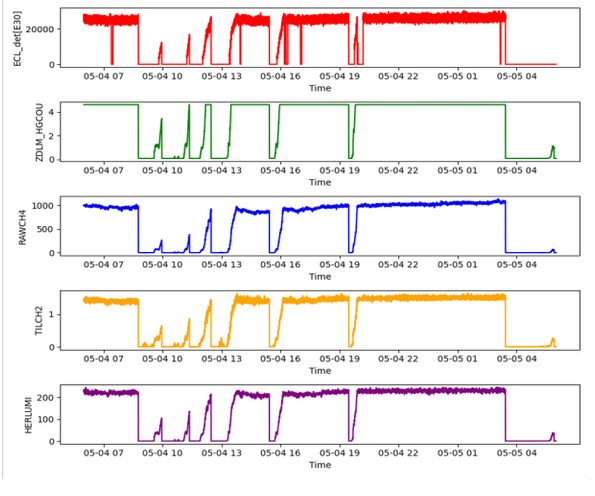

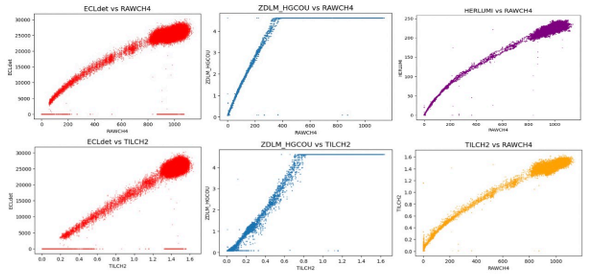

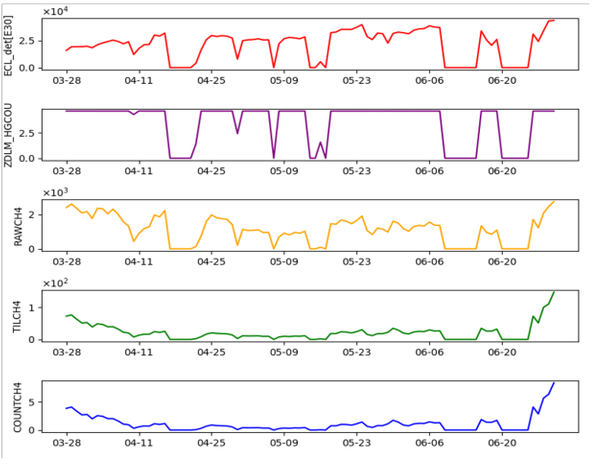

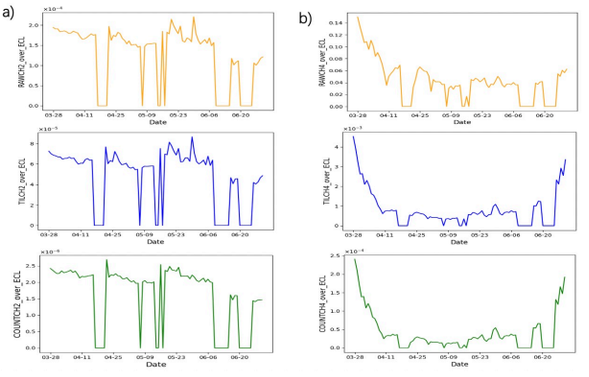

- **Bunch integrated luminosity signals**

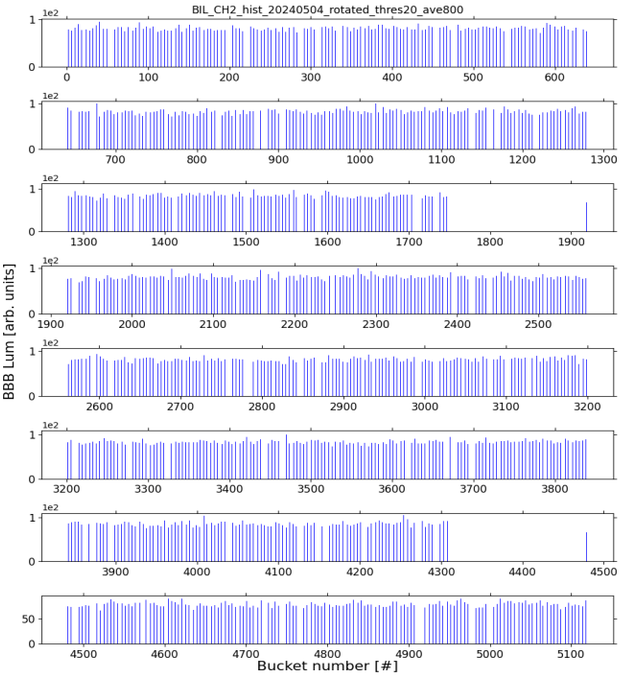

Conclusion

The LumiBelle2 fast relative luminosity monitor of SuperKEKB operated successfully during the 2024ab run, providing useful signals for the tuning of the beams at the IP. A number of questions will have to be studied for the next runs, especially radiation damage issues for the diamond located nearest to the tungsten radiator in the LER, as well as a number of improvements to the data acquisition and data handling software.

Poster ID:301 The 2024 International Workshop on the High Energy Circular Electron Positron Collider

CEPC stereo ECAL muon momentum reconstruction

Lei Guo[1], Huaqiao Zhang[2], Shengsen Sun[2], Han Wang[2], Yongsheng Huang[1], Yang Liu[1]

1. Sun Yat-sen University

2. The Institute of High Energy Physics of the Chinese Academy of Sciences

guolei23@mail2.sysu.edu.cn

Hangzhou, Oct 23-27, 2024

Introduction

This research focuses on the particle reconstruction algorithm of the **stereo crystal electromagnetic calorimeter** (stereo ECAL) for the CEPC. The stereo crystal structure, as one of the design options for the CEPC ECAL, possesses unique properties. It not only provides information on the energy deposition but also reconstructs 3D cluster information from 2D plane information with minimal dead zones.

Layout of CEPC stereo ECAL and Hitmap

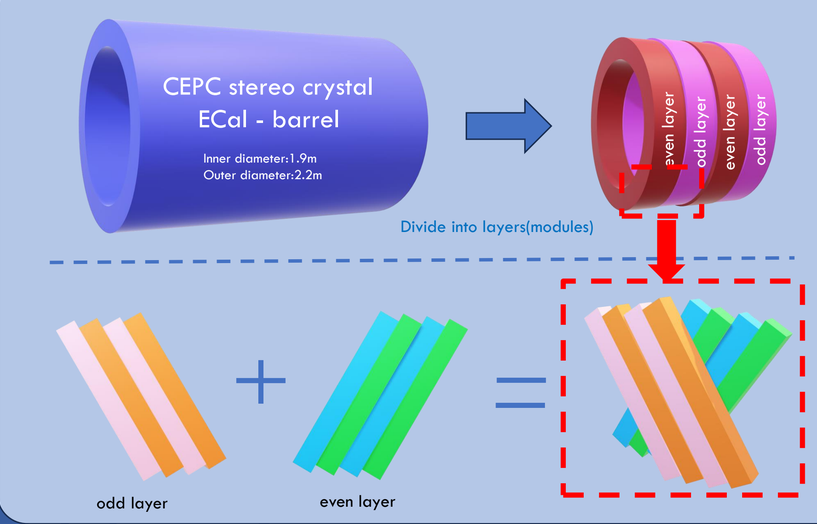

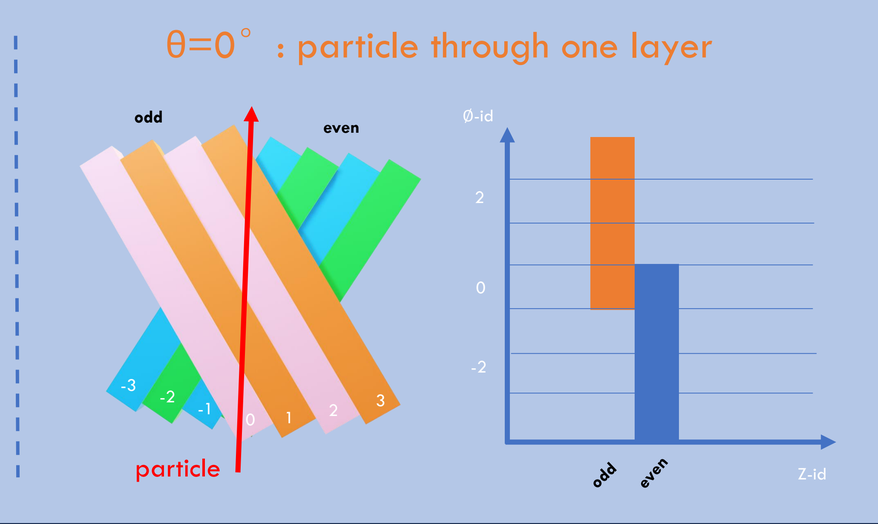

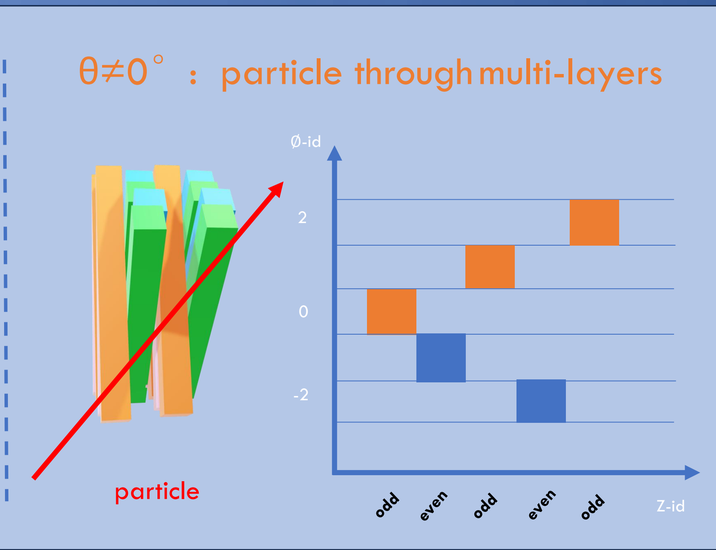

Reconstruct the charge info

The direction of the opening helps us determine the charge. Energy threshold is 2 MeV for this study.

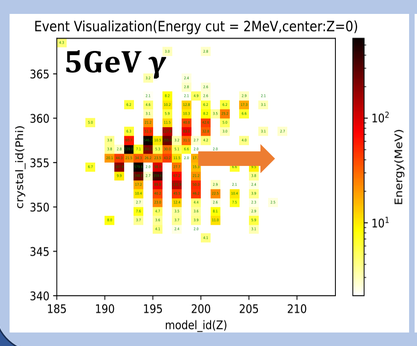

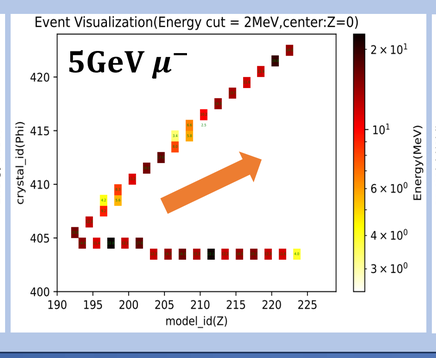

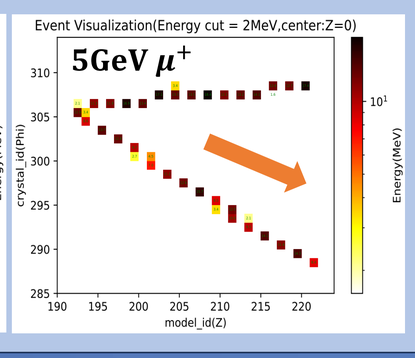

type	γ(left)	μ^-(medium)	μ^+(right)
rad(β)	-0.02	0.26	-0.26
degree(β)	-0.99° →	14.86° ↗	-14.66° ↘
charge	0	-1	1

β is the relative deflection angle of the motion

Reconstruct the P_T info

This research analyzes the energy deposition distribution of single muon events within the stereo ECAL up to 10 GeV Based on the motion of charged particles in a magnetic field, the relationship between β and P_T is derived.

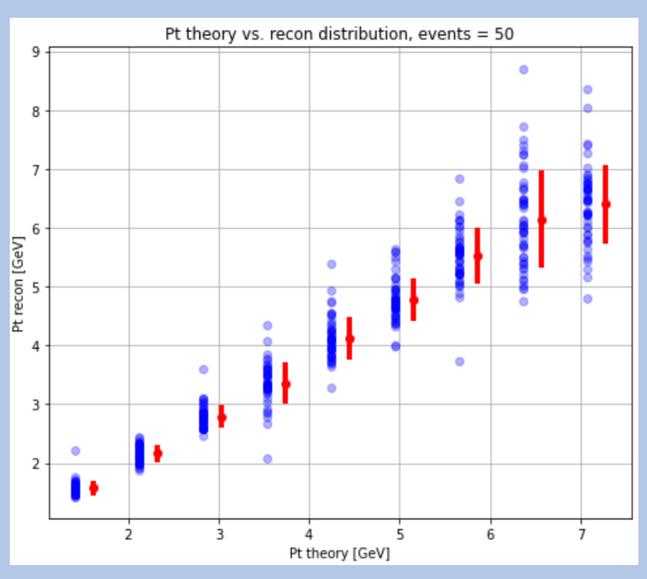

$$P_T = 0.15BL\frac{1}{\sin(\beta)}$$

9 Single μ^-, θ=45° ,Φ=100° Samples:

- P: 2,3,4,5,6,7,8,9,10 GeV
- Statistic for each P : 50 events
- Energy threshold: 2MeV
- $P_T = P/\sin(\theta) = P/\sqrt{2}$
- $B = 3\mathrm{T}$, $L = 1.9\mathrm{m}$
- $\sigma = \frac{(P_T\_\text{reco} - P_T\_\text{theory})}{P_T\_\text{theory}}$

Summary & Conclusion

- Layout of CEPC stereo ECAL and Hitmap
- Preliminary study on CEPC stereo ECAL muon momentum reconstruction
  - Reconstruct the open angle
    → obtain the charge info
  - Obtain the relation between P_T and β
    → obtain the momentum info
  - Plot of P_T and σ $\left(\sigma = \frac{(P_T\_\text{reco} - P_T\_\text{theory})}{P_T\_\text{theory}}\right)$
    → σ study, mostly $\Delta P_T/P_T$ <20%

THANKS FOR YOUR ATTENTION !

Poster ID:338

Design for the Spiral Barrel Yoke of CEPC Detector: A Self-Supporting Installation Scheme

Shang Xia, Quan Ji, Yujie Li ——IHEP

Abstract

Leveraging the spiral structure of the CEPC detector barrel yoke, we have designed an innovative installation scheme. This scheme comprises three primary parts: the barrel yoke module, end flange, and barrel yoke support structure. By dispensing with the auxiliary installation structure traditionally used, the barrel yoke can be installed utilizing its own end flange, thereb y streamlining the installation process. The design of the end flange also significantly enhances the structural strength of the barrel yoke. Furthermore, this installation scheme minimizes material waste and optimizes the use of underground space.

Detailed Structure

Barrel yoke structure design

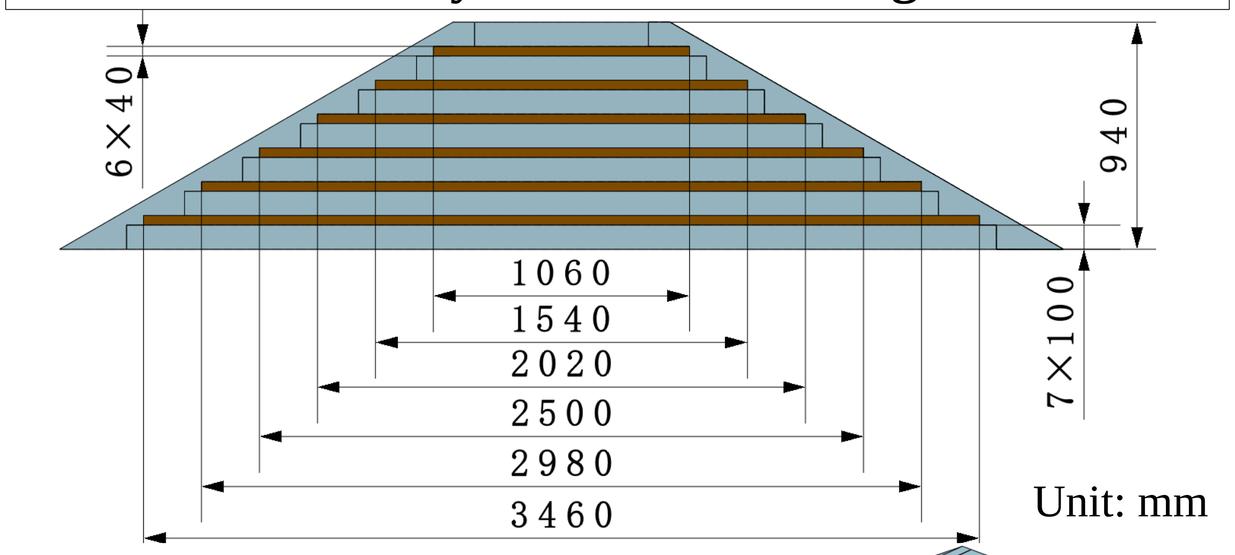

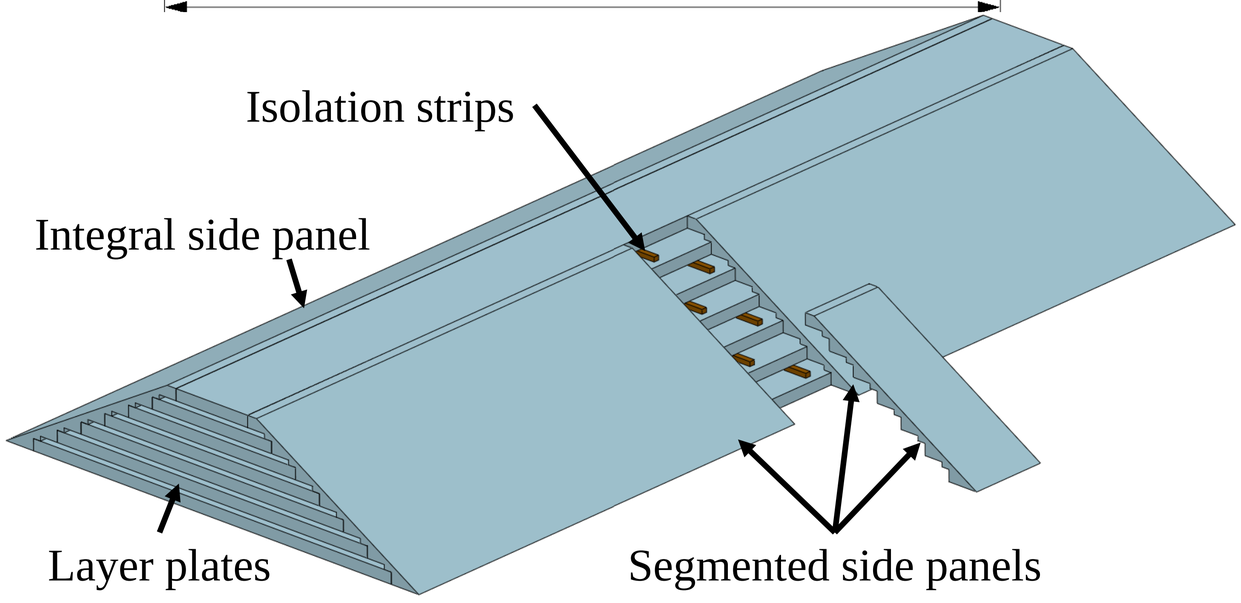

Design: dodecagon structure with 12 modules
Layer plates: 7 layers, 100mm / each
Muon detector space: 6 layers, 40mm / each
Feature: The width of the spiral module is gradually reduced from the inside to the outside of the barrel yoke. The spiral module can open the segmented side panels for installation and maintenance of the muon detectors without disturbing the internal detectors.

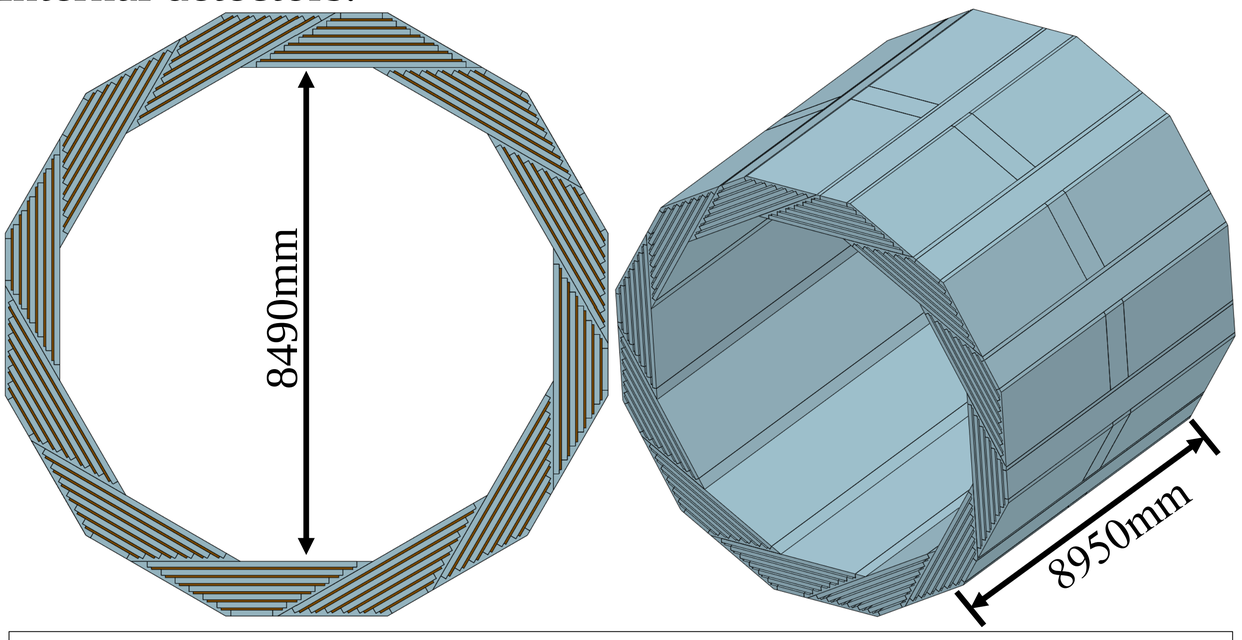

Barrel yoke installation design

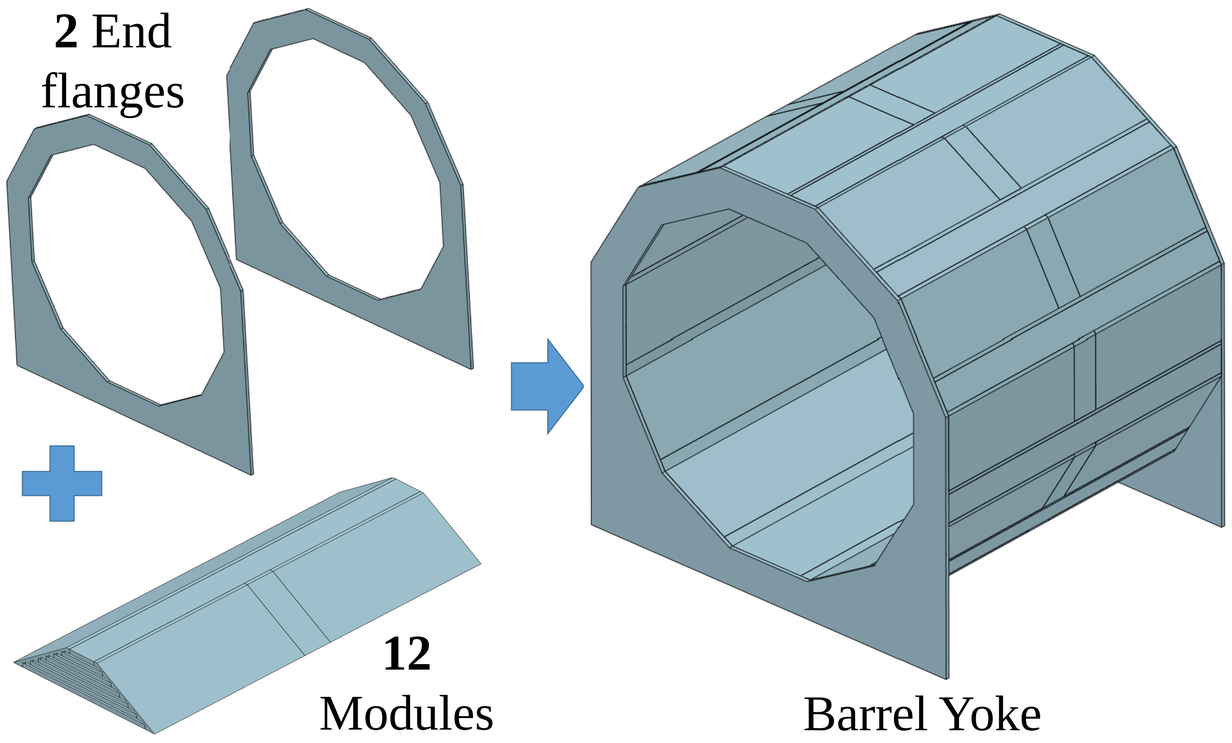

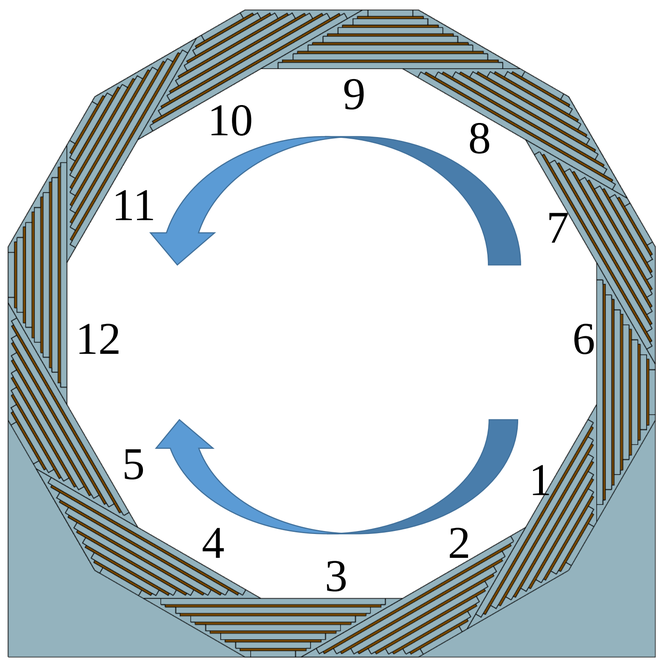

Installation method:
Both ends of module can be fix ed to end flanges. Then comple te the installation of the barrel yoke module according to the installation sequence shown on the left. The end flanges is part of the barrel yoke, which does not need to be removed, nor do es it require additional auxiliar y installation structure, and no material waste.

Barrel yoke simulation & optimization

Deformation of end flanges of gravity — Unit: mm

Sequence	1	2	3	4	5	6	7	8	9	10	11	12
Flange deformation	0.12	0.12	0.12	0.12	0.18	0.26	0.32	0.66	1.13	1.27	1.29	1.07

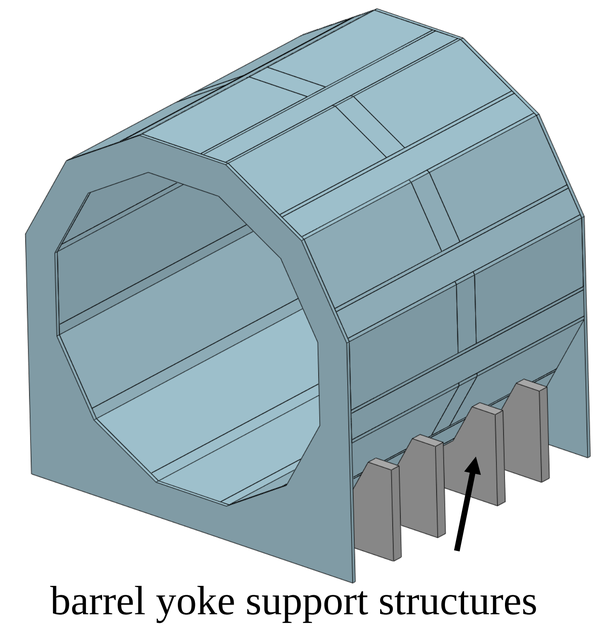

barrel yoke support structures

Key: The end flanges will be deformed during the installation of module. When the top modul es of the barrel yoke is installed, the deformation is large, which may affect the installation of subsequent module.
Optimization: Support the bottom modules to reduce end flanges deformation.

Deformation of end flanges of gravity (optimized) — Unit: mm

Sequence	1	2	3	4	5	6	7	8	9	10	11	12
Flange deformation	0.11	0.11	0.11	0.11	0.11	0.13	0.15	0.45	0.88	1.01	1.02	0.80

Barrel yoke simulation results of self-weight

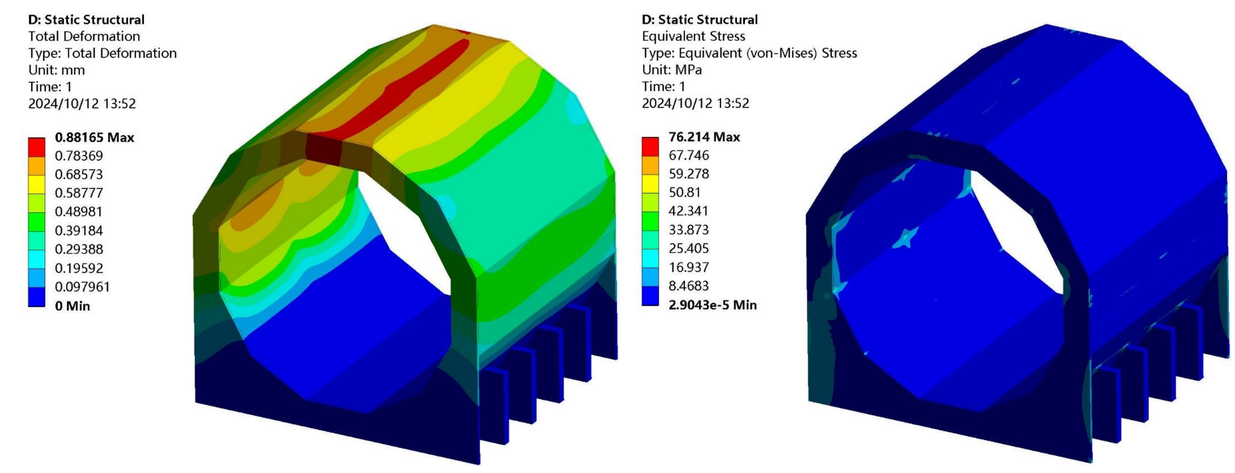

Deformation max
0.88mm

Equivalent Stress max
76.21MPa

Conclusion: After supporting the bottom modules of the barrel yoke, deformation of the end flanges is reduced during the module installation. The addition of barrel yoke support structures is more conducive to the installation of the barrel yoke module. It also increases the strength of the barrel yoke. From the simulation result, we can also enhance the accuracy of installation and minimize the risks associated with installa tion. Subsequently, the barrel yoke support structure and end flange structure will be optimized continually.

Comparing Event Generators for Radiative Bhabha Interaction at CEPC

Jiading Gong[1] Weimin Song[1] Renjie Ma[2] Lei Zhang[2] Haoyu Shi[3] Suen Hou[4]
[1]Jilin University [2]Nanjing University [3]Institute of High Energy Physics, CAS
[4]Institute of Physics, Academia Sinica

Abstract

Small-Angle Bhabha Scattering is a traditional process used for high-precision luminosity measurement at electron-positron colliders, known for its clean event signature and large cross section. The Circular Electron Positron Collider (CEPC) is a Higgs factory that will produce millions of HZ events at $\sqrt{s} = 240\text{GeV}$, and 0.7 trillion Z bosons at the Z-pole energy. In order to improve precision on measurements of Standard Model processes, the luminosity systematic with an accuracy of 10^{-4} is required. This study focuses on the measurement of radiative Bhabha interaction using the event generators ReneSANCe and BHLUMI, aiming to achieve a systematic uncertainty of 0.01% for the Bhabha cross-sections. The radiative photons from NLO processes are compared in terms of momentum and opening angles relative to the electrons, considering the luminometer acceptance at CEPC.

Introduction

The cutting-edge methods for calculating luminosity theoretically using BabaYaga [1] and BHLUMI [2] have been identified as the most advanced codes. The Monte Carlo (MC) BHLUMI generator, which is solely based on QED principles, has a theoretical uncertainty of around 0.037% (refer to Table 2 in [3]). The study also outlined the potential for achieving a theoretical precision of 10^{-4} in future collider experiments at the Z peak for luminosity measurements.

The latest version of BabaYaga now includes considerations for a range of radiative corrections, such as QED, (electro)weak, and higher-order effects. This generator is primarily designed for large-angle Bhabha scattering, with theoretical uncertainties estimated to be around 0.1% [4]. As our study focused on Small-Angle Bhabha Scattering (SABS), we opted not to utilize the BabaYaga generator.

Besides, we also made use of the Monte Carlo event generator RenSANCe (Renewed SANC Monte Carlo event generator) in our research. This generator provides a precise electroweak (EW) description at next-to-leading order (NLO) for important processes at electron-positron colliders, considering polarization effects [5].

The poster is structured as follows. In the section "SABS cross sections" we compared the numerical results for the cross sections with MC generator BHLUMI and ReneSANCe. In the section “Angular distributions," we discussed angular event distributions of experimental significance and analyzed the impact of the minimum cut-off on the electron scattering angle with MC generator ReneSANCe.

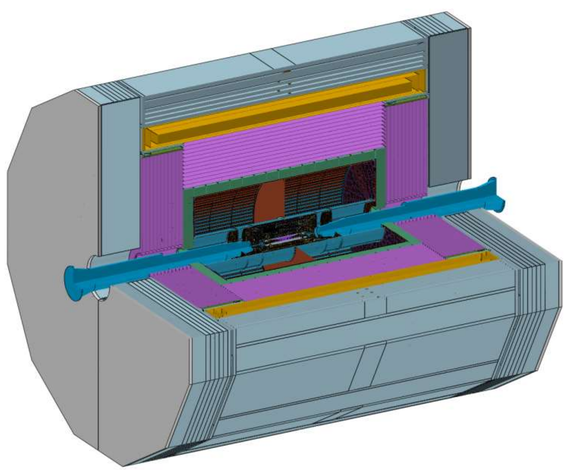

Figure 1. The conceptual design of CEPC detector.

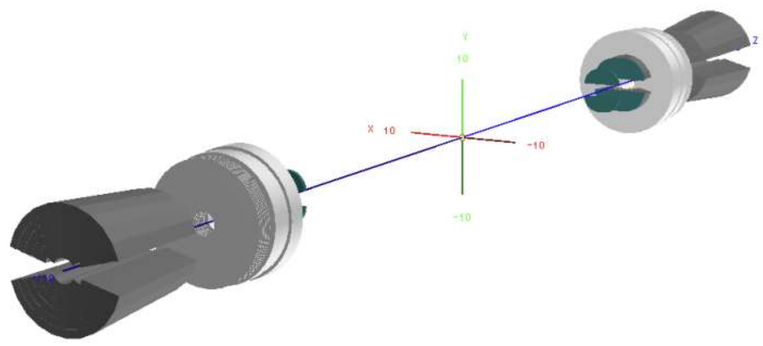

Figure 2. The geometry of LumiCal.

SABS cross sections

The results were obtained within the $\alpha(0)$ electroweak scheme. Additionally, the luminosity acceptance was set at $\theta > 30$ mrad (1.72 degrees).

In order to showcase the capabilities of the two programs, we generated 1 million events for the Bhabha cross section at center-of-mass (c.m.s.) energies ranging from 100 GeV to 300 GeV. The results are presented in Table 1 and Figure 5.

```
# Process id:
pid : 101
    # 101 - e^+e^-  --> e^-e^+
    # 102 - e^+e^-  --> ZH
    # 103 - e^+e^-  --> mu^-mu^+
    # 104 - e^+e^-  --> tau^-tau^+
#!!!!!!!!!!!!!!!!!!!!!!!!!!!!!!!!!!!!!!!!!!!!!!!!!!!!!!!!!!!!!!!!!!!!!!!
# ALR:
alr  : 0
    # 0 - sigma, 1 - sigma_RL-sigma_LR, 2 - sigma_RL+sigma_LR,
    # 3 - sigma_0L-sigma_0R, 4 - sigma_0L+sigma_0R
#!!!!!!!!!!!!!!!!!!!!!!!!!!!!!!!!!!!!!!!!!!!!!!!!!!!!!!!!!!!!!!!!!!!!!!!
# Longitudinal polarization of initial particles:
lamep :    0 # e^+ polarization
lamem :    0 # e^- polarization
#!!!!!!!!!!!!!!!!!!!!!!!!!!!!!!!!!!!!!!!!!!!!!!!!!!!!!!!!!!!!!!!!!!!!!!!
# EW scheme:
gfscheme : 0
 # 0 - alpha(0)
```

Figure 3. Example ReneSANCe settings file.

```
prod2 prod2 llog2 obis2   =========Data set for BHLUM2 test=========
 0 1 0 0 0 0 0 0    KAT1,KAT2,KAT3,KAT4,KAT5,KAT6,KAT7,KAT8
   1000000      NEVT
      3001      KEYOPT = 1000*KEYGEN +100*KEYREM +10*KEYWGT +KEYRND
      1022      KEYRAD =              100*KEYUPD +10*KEYMOD +KEYPIA
         2      KEYTRI  Obsolete!!!
     2.0D0      CMSENE
       .03      Tming   theta_min [rad]    genaration
1.57079633      Tmaxg   theta_max          generation
  0.9999D0      VMAXG   v_max              generation
      1D-5      XK0     eps_CMS            generation
      .024      TminW   theta_min sical    trigger wide
      .058      TmaxW   theta_max sical    trigger wide
      .024      TminN   theta_min          trigger narrow
      .058      TminN   theta_max          trigger narrow
     0.5D0      VMAXE   v_max              trigger maximum v
        32      NPHI    nphi      sical    trigger no of phi   sect.
        16      NTHE    ntheta    sical    trigger no of theta sect.
================= the end of data set BHLUM2 ================
```

Figure 4. Example BHLUMI settings file.

Table 1. The cross section.

$\sqrt{s}$, GeV	σ, nb (ReneSANCe)	σ, nb (BHLUMI)
100	120.33(3)	120.59(8)
120	83.80(2)	84.14(5)
140	61.75(2)	61.96(4)
160	47.37(1)	47.58(3)
180	37.50(1)	37.67(2)
200	30.42(1)	30.59(2)
220	25.19(1)	25.34(2)
240	21.19(1)	21.32(1)
260	18.08(1)	18.20(1)
280	15.62(1)	15.71(1)
300	13.61(1)	13.71(1)

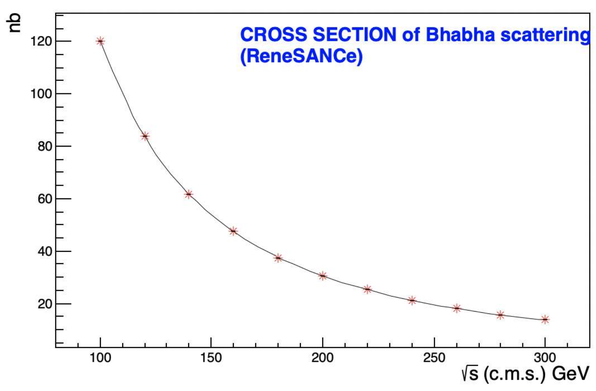

Figure 5. Variation of the cross section with c.m.s..

Angular distributions

Next, we examined the distribution of lepton scattering angles between the outgoing and incoming positrons, as well as the distribution based on the angle at which the photon was emitted.

We generated 1 million Bhabha events at $\sqrt{s} = 240\text{GeV}$ for the acceptance of the luminometer $\theta > 30$ mrad (1.72 degrees). The sharp edges at 1.72 degrees correspond to the acceptance limits of the luminometer. The results are shown in Figure 6-8.

And then we set the range of luminosity measurement from 30 mrad to 174.5 mrad, and assumed electrons were allowed to scatter by any angle, down to zero. We discovered that the total fraction of events within the angular range of (0, 30) mrad for θ_{14} is approximately 1-2 permille. In the angular range of (0, 10) mrad, the relative event yield is about less than 10^{-4}.

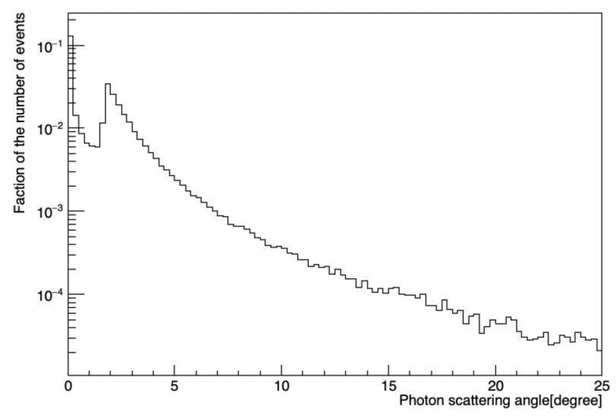

Figure 6. Angular distribution θ_{15} between the initial positron p_1 and the photon p_5 .

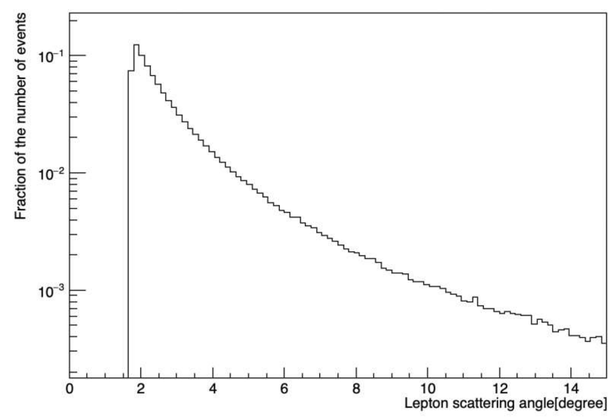

Figure 7. Angular distribution θ_{14} between the initial positron p_1 and the final positron p_4 .

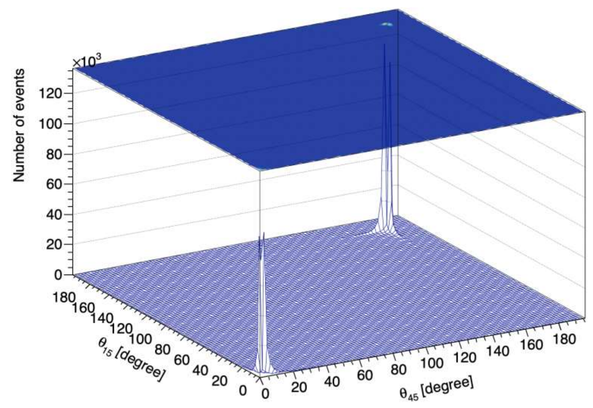

Figure 8. Angular distribution θ_{45} vs θ_{15}, indicating FSR and ISR photons with small opening angles to p_4 and p_5, respectively.

Conclusions

We utilized the BHLUMI and ReneSANCe generators to simulate small-angle Bhabha scattering. Comparisons of scattering cross sections were made at the luminosity acceptance greater than 30 mrad, and the results from both generators showed a rough match. We plan to further optimize the parameter settings of the two programs. In terms of studying the angular distribution, we exclusively employed the ReneSANCe generator and intend to extend this analysis to BHLUMI. Detailed statistics on the fraction of the number of events at the lepton scattering range of (0, 30) mrad and (0, 10) mrad with the acceptance of the luminometer (30, 174.5) mrad will be conducted. Our study suggests that the detection of Small-Angle Bhabha Scattering events is a viable approach to achieving a precision of 10^{-4} for the luminosity measurement at CEPC.

Contact

Jiading Gong
Jilin University
Email: gongjd23@mails.jlu.edu.cn

References

[1] G. Balossini, C. Bignamini, C. Carloni Calame et al., Phys. Lett. B **663**, 209 (2008)
[2] S. Jadach, W. Placzek, E. Richter-Was et al., Comput. Phys. Commun. **102**, 229 (1997)
[3] S. Jadach, W. Płaczek, M. Skrzypek et al., Eur. Phys. J. C **81**, 1047 (2021)
[4] C. M. Carloni Calame, G. Montagna, O. Nicrosini et al., edited by A. Denig and C. F. Redmer, EPJ Web Conf. **218**, 07004 (2019)
[5] R. Sadykov and V. Yermolchyk, Comput. Phys. Commun. **256**, 107445 (2020)
[6] A.B. Arbuzov, S.G. Bondarenko, I.R. Boyko et al., Chin. Phys. C **48**, 043002 (2024)

Poster ID: 351

Fast Luminosity Diamond Monitor for CEPC

Jialiang Zhang[1,2], Suen Hou[3], Ming Qi[1,2], Lei Zhang[1,2]

[1] School of Physics, Nanjing University, Nanjing, China
[2] National Laboratory of Solid State Microstructures, Nanjing University, Nanjing, China
[3] Institute of Physics, Academia Sinica, Taipei, Taiwan

Introduction

A fast luminosity monitor using diamond strip detectors is proposed to detect small-angle Bhabha scattering electrons from e^+e^- collisions at 10 mrad (in the CMS frame), boosted by 33 mrad due to beam crossing (CMS +16.5 mrad in the lab frame). It is designed to be placed in the MDI volume, close to the beam-pipe wall along the lab frame's boosting direction. Multiple electronic-grade diamond strips will be integrated into a diamond slab detector, positioned in front of the quadrupole at $|z|$ = 855~1110 mm, with x = – 27 mm and y from – 12 to 12 mm beside the beam-pipe. By measuring symmetric event rates on the $-z/+z$ sides, it will monitor luminosity at a high rate. It will also provide real-time feedback on interaction point (IP) offsets in the z and y directions, based on the shower profile in diamond slab from Bhabha scattering electrons.

Fast Luminosity Diamond Monitor

Two diamond slabs are designed to be installed close to the beam pipe, represented as yellow blocks in Figure 1:

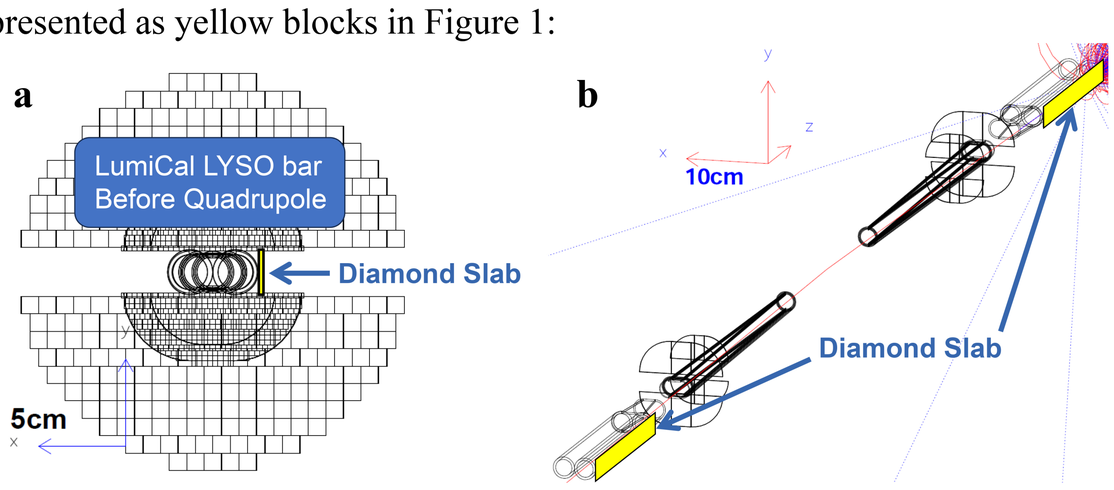

Fig. 1a: x-y view of the Diamond at x=-27mm between the LumiCal detector of LYSO bars in 10×10 mm² blocks. The project of LumiCal in front of Flange are also projected. 1b:The MDI is shown with a race-track pipe, the LumiCal Si-wafers, and the Diamond slabs on the side of the boost direction.

Each diamond slab is composed of dozens of diamond strip electrodes stitched together, segmented with a 2 mm pitch to measure Bhabha electron showers passing through the 3 mm thick Cu beam-pipe. Schematic diagram and specific location coordinates are shown in Figure 2:

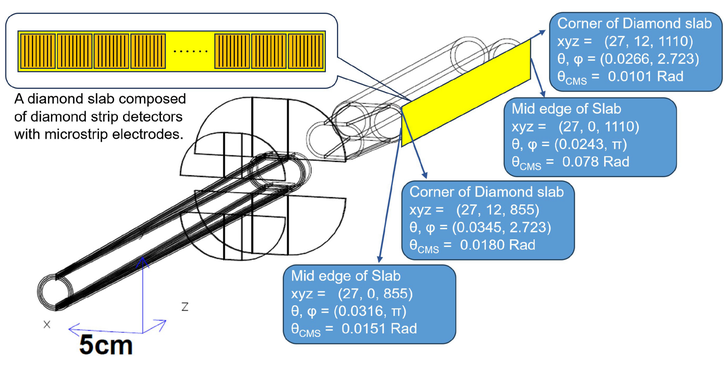

Fig. 2: The coordinates of the diamond slab and the preliminary layout of the diamond strip electrodes. The strip electrodes can be arranged in different orientations.

Shower profile, Sensitivity to θ and IP offset

The Bhabha cross sections covered by the diamond detector are estimated to be on the order of 100 nb, corresponding to a trigger rate of 100 kHz at an instantaneous luminosity of $1\times10^{36}/cm^2\cdot s$. Simulations of the shower profile for a 50 GeV electron at θ = 10 mrad (CMS), boosted to 26.5 mrad in the x-direction passing through the copper beam pipe and hitting the diamond, are presented in Fig. 3a. For comparison, shower profiles for electrons at 9 to 12 mrad are also displayed in Fig. 3b. The fast monitoring functionality can be achieved with several thousand diamond strips, each with a 2 mm pitch, and a 100 kHz readout system.

The sensitivity of diamond shower profiles to interaction point (IP) offsets has also been simulated. An IP offset in the x-direction is equivalent to a shift in θ, which is not detectable. However, offsets in the y and z directions can be obtained through the cross-sectional patterns of the shower in different directions. With a 2 mm strip pitch, the diamond detector is sensitive to an angular resolution of 0.1 mrad, and can detect IP offsets of 0.1 mm in the y-direction and 1 mm in the z-direction.

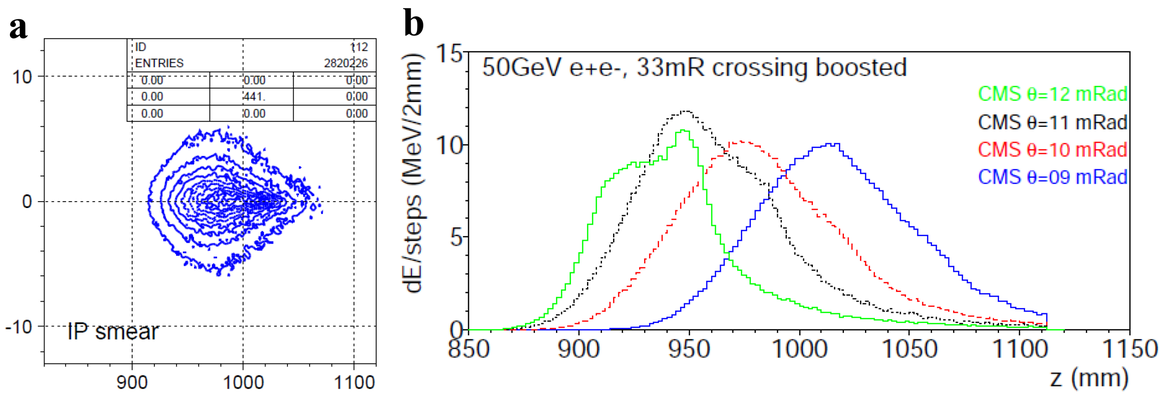

Fig. 3a: for a 50 GeV electrons at θ= 10 mRad (CMS), boosted in x at 26.5 mRad. 3b: Comparison of shower profiles on diamond at 9 to 12 mRad.

Fabrication of Diamond sensors

Based on the research for calorimeters in the forward region of the HL-LHC-ATLAS, high-quality, electronic-grade single-crystal diamond sensors have been fabricated at Nanjing in collaboration with various institutions. The diamond materials were synthesized using 30 kW direct current (DC) arc plasma chemical vapor deposition (CVD), and metal electrodes were deposited onto the diamond surface through magnetron sputtering. The resulting single-crystal diamond sensors have a thickness of 300-500 μm and a surface area around 0.5 cm². The sensors are mounted on a ceramic-based high-frequency Rogers board, providing secure support for the diamond and facilitating effective integration with the readout electronics. They achieve a dark current in the range of tens of picoamperes at an electric field of 2.5 V/μm, resulting in a high signal-to-noise ratio.

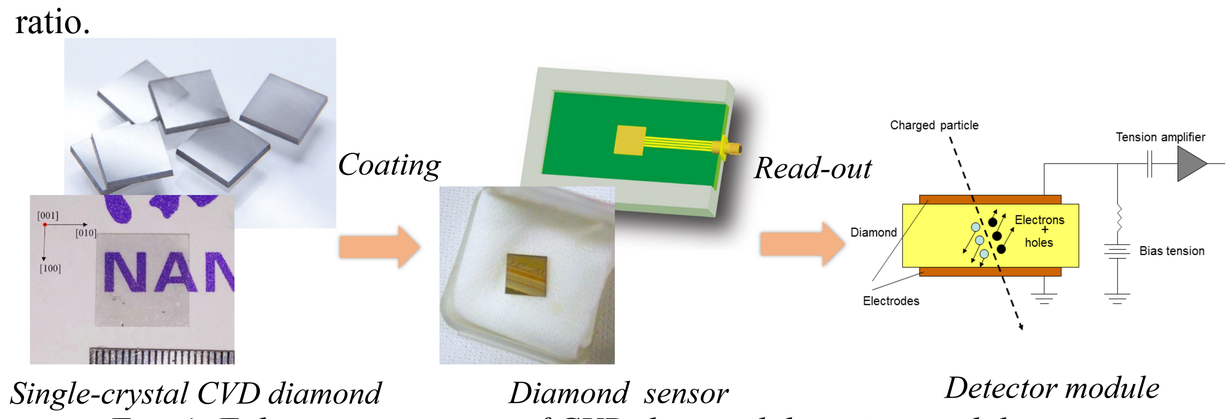

Fig. 4: Fabrication process of CVD diamond detecting module

Radiation tolerance test of diamond sensor

- Fast neutron irradiation was conducted at the IBR-2M reactor in Dubna, Russia, with a total of 280 hours, a total dose of 3.3×10^{17} n/cm²;
- 100 MeV proton irradiation was conducted at CIAE for a total of 47 hours, accumulating a dose of 1.6×10^{17} p/cm²;
- Radiation tests reveal that, at an expected radiation level of 3×10^{17} n/cm² (~10 MGy), diamond sensors demonstrate the ability to maintain low noise operation and signal attenuation can be corrected through calibration.

Electrodes design on Diamond sensor

To meet the requirements for fast luminosity and IP offset monitoring, diamond sensors have been designed with microstrip electrodes. Advanced electrode techniques are also being explored to further improve resolution.

Microstrip Electrodes :

- Microstrip electrodes with a width of 1 mm (and a minimum achievable of
- 10 μm) can be fabricated through photolithography and coating techniques.
- Readout strip could be directly wire bonded from the diamond strip detector to a VA2.2 readout channel;

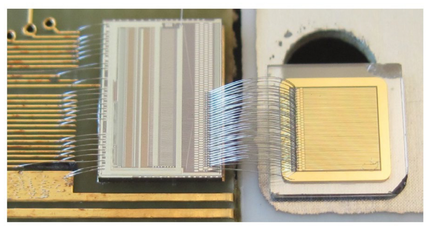

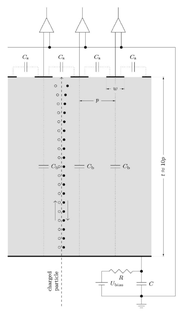

Fig. 5: Schematic diagram of a 50 μm pitch diamond microstrip detector prototype[1] and its principle.

3D Electrodes :

- Proposed scheme for fabricating cutting-edge 3D electrodes in diamond;
- Utilizing femtosecond pulsed laser to induce the transformation of the sp^3 phase in diamond to a conductive sp^2 phase, serve as the electrodes;
- Improves both time and spatial resolution by 30%;
- Enhancing radiation resistance by improving CCE.

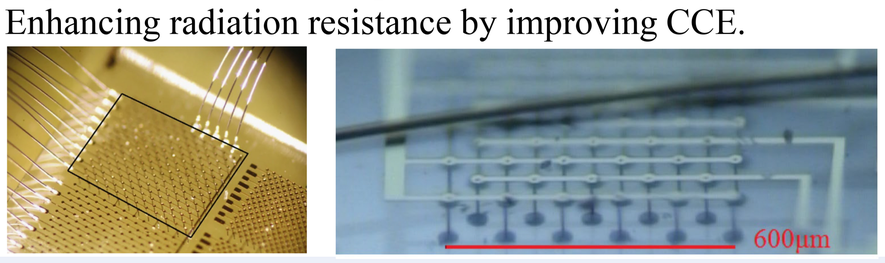

Fig. 6: 3D electrodes[2] inside the diamond bulk

Conclusion

By integrating radiation-resistant diamond sensors with a pitch of 2 mm or less, a diamond slab positioned adjacent to the beam pipe can facilitate fast luminosity monitoring through real-time feedback on event rates from the –Z and +Z sides. Additionally, with pattern recognition, the system can achieve a resolution of 0.1 mRad for detecting scattered electrons, a resolution of 1 mm for shifts in the interaction point (IP) in the z direction, and 0.1 mm for shifts in the y direction, given an appropriate electrode configuration. The production of diamond materials and various advanced electrodes can be conducted in laboratories in Nanjing.

References

[1] CERN RD42, J. Phys. D: Appl. Phys. 52 (2019) 465103
[2] CERN RD42, 38th International Conference on High Energy Physics

Contact info: jlzhang@smail.nju.edu.cn (Jialiang Zhang); suen@sinica.edu.tw (Suen Hou)
The 2024 International Workshop on the High Energy Circular Electron Positron Collider